UNIVERSITY OF OKLAHOMA

GRADUATE COLLEGE

DIGITAL RADAR IMPLEMENTATION WITH SYSTEM RESPONSE COMPENSATION THROUGH AMPLITUDE PREDISTORTION

A THESIS

SUBMITTED TO THE GRADUATE FACULTY

in partial fulfillment of the requirements for the

Degree of

MASTER OF SCIENCE

By

BRIAN M. SUN
Norman, Oklahoma
2016

DIGITAL RADAR IMPLEMENTATION WITH SYSTEM RESPONSE COMPENSATION THROUGH AMPLITUDE PREDISTORTION

A THESIS APPROVED FOR THE
SCHOOL OF ELECTRICAL AND COMPUTER ENGINEERING

BY

Dr. Mark Yeary, Chair

Dr. Caleb Fulton

Dr. Nathan Goodman

This work is dedicated to my family, my fiancèe and my friends. Without their support and encouragement this work would not have been possible.

Acknowledgments

I'd like to thank Dr. Yeary for his advisement and diligence in this work as well as my committee members Dr. Goodman and Dr. Fulton for their support, being great sounding boards, and sources of guidance. I'd also like to thank Dr. Faruk Uysal for being a great mentor and motivator for this project.

Table of Contents

List of Tables

List of Figures

Abstract

Radars traditionally synthesize waveforms by using a variety of analog electronics. These analog components are collectively referred to as the analog chain. A typical electronic analog chain contains multiple components, such as frequency mixers, signal generators and local oscillators. The analog chains are typically used in radars for both the transmit and receive circuits. This design generally causes radars to be unnecessarily bulky and power intensive.

However, with modern advancements in digital electronics, waveforms can more easily be synthesized and captured using only digital electronics. Digital electronics require significantly less power and occupy less space. The synthesis of radar waveforms using only digital electronics, such as Digital-to-Analog Converters (DACs) and Analog-to-Digital Converters (ADCs), allows for a majority of the analog chain to be removed from the system. A single digital component requires less power and provides more capability, thus providing a better alternative to the typical analog chain. In addition, digital signal processing techniques can still be used to increase the efficiency of the radar system. For instance, the received signal can be under sampled to reduce the amount of data collected by the radar.

The effects of the system response cause the amplitude modulus of the waveform to be inconsistent, which effectively causes fluctuations in the power transmitted by the radar. Having a radar waveform with fluctuations in transmitted power is not ideal since the range of the radar is a function of the power transmitted. When implementing pulse compression signal processing, a waveform with a fluctuating modulus reduces the signal-to-noise ratio returned from the matched filter. In applications like Synthetic Aperture Radar (SAR), having a high signal-to-noise ratio is crucial to creating an accurate image. In order to create a constant amplitude waveform, the amplitude distortions must be compensated for. The method utilized here

to compensate for the amplitude distortions is to predistort the waveform. When the predistorted waveform is influenced by the system, the output waveform has a near constant amplitude modulus.

1 Intoduction

Radars are used in a number of modern day applications ranging from defense systems to imaging terrain and enforcing highway speed limits. Radars are also used in the current day automotive industry [1]. The broad range of applications for radar result in multiple different configurations of radar. Radars need three major components to function: the transmit chain, the receive chain, and the processing computer [2]. The transmit chain is required to create and propagate the waveform through the air. The receive chain collects the waveform that is reflected back from objects. Lastly, the processing computer interprets the waveform collected and attempts to extract the desired data. Currently, digital radars are growing in popularity, specifically in phased array radars. Phased array radars traditionally require each element of the array to have their own respective excitation circuits. Most phased array radars are designed with a calibration stage where the waveforms are manipulated to ensure the effects of mutual coupling and other element distortions are mitigated [3]. The predistortion technique described in this paper can also be used in phased array applications. For instance, a SAR system that performs beam steering can utilize the technique to ensure all beams have a constant modulus. The system designed and used in this paper was modeled after the EcoSAR system developed by NASA [4]. The EcoSAR system utilizes independent loopback calibration tests for each transmit and receive element [5]. The predistortion technique discussed in this paper is designed to utilize these loopback tests to generate a waveform with a constant modulus. Furthermore, the predistortion technique proposed can be inplemented on low cost systems utilizing field programmable gate arrays (FPGAs) like those described in [6]. Moreover, multiple input multiple output (MIMO) radar systems, like the one described in [7][8], could also benefit from the predistortion technique. Another common application is a continuous

wave radar, which utilizes a continuously propagated waveform to detect the distance to the target. Continuous wave radars have multiple configurations in just the waveform alone. For instance, the waveform could either be modulated or just a single tone. Another application is a form of speed enforcement radar that utilizes a pulsed waveform. When the officer presses a button, the systems begins sending pulses and the target's speed is derived from the phase change or Doppler shift between pulses. However, even though radars have a wide variety of implement, the key components of a radar remain the same.

Even in the components of a radar, the variations that can be utilized are extensive. Completely analog configurations use analog devices to create the signal. These configurations utilize oscillators to create a sinusoidal wave. Analog systems then utilize additional devices to convert the signal to the desired frequency. Radars operate in multiple different frequency regions within the radio frequency spectrum. Each band of frequency is designated by the Institute of Electrical and Electronics Engineers (IEEE) [9]. Table 1.1 shows the designations as displayed in the IEEE standard. In addition, analog filters are used to remove unwanted components of the signal. The main limitation of analog devices is that modulated signals cannot be created easily. The solution to easily creating modulated signals is to create the signal digitally. Digital radar configurations use digital electronics to synthesize the waveforms. The digital electronics create the signal by producing samples in rapid succession that, when interpolated, behaves like an analog signal. Digital electronics allow for floating point operations, which allow for the values of the samples to be calculated with more extensive methods. Most importantly, as described in this thesis, the digital electronics can also be used to correct the shortcomings of the analog components.

Table 1.1: IEEE Defined Frequency Bands

Band Label	Minimum Frequency	Maximum Frequency
HF	3 MHz	30 MHz
VHF	30 MHz	300 MHz
UHF	300 MHz	1000 MHz
L	1 GHz	2 GHz
S	2 GHz	4 GHz
C	4 GHz	8 GHz
X	8 GHz	12 GHz
Ku	12 GHz	18 GHz
K	18 GHz	27 GHz
Ka	27 GHz	40 GHz
mm	40 GHz	300 GHz

The methods allow for creating samples that represent more sophisticated signals. In addition, the method allows for any signal that can be represented mathematically to be represented by a set of discrete digital samples. Digital electronics also allow for some of the analog components to be replaced by a single digital component.

1.1 Matched Filter

Most radar applications transmit a waveform and listen for the reflections off of a target of interest. Assuming the reflections of the waveforms are not altered in a non-linear fashion, the radar can anticipate the waveform that it will be receiving. The received data can be processed so that the radar only shows a detection when the expected waveform is received. This processing technique leads to the creation

of a *matched filter*. A matched filter is a filter that is designed to specifically filter out everything but the expected waveform. However, the filter does not actually remove the waveform from the unwanted, noisy received data. Instead, the filter maximizes the signal-to-noise ratio (SNR) of the desired received waveform. This is because filters in linear systems are applied through convolution, as shown in Figure 1.1.

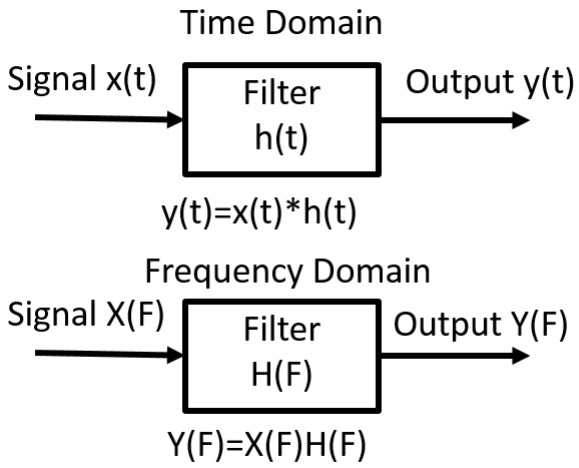

Figure 1.1: Linear System Representation of a Filter

The filter must be constructed so that when the received waveform is convolved with the filter a higher SNR occurs. In order to increase SNR, the power of the signal must be increased by the matched filter. Using equation (1.1), the estimated signal power is the magnitude of the sum of time domain signal squared. The following derivation can be seen in detail in [10]. The power of the signal is computed first:

$$P = |x(t)|^2 \ , \tag{1.1}$$

with P equal to the signal power and $x(t)$ defined as the time domain signal. Utilizing the inverse Fourier transform and the frequency domain signal model in Figure

1.1, the time domain representation of the output after the matched filter becomes equation (1.2). Placing the time domain signal output of the matched filter into equation (1.1), the power from the output of the matched filter can be calculated as shown in equation (1.3):

$$y(t) = \frac{1}{2\pi}\int_{-\infty}^{\infty} X(F)H(F)\mathrm{e}^{j2\pi Ft}dF \tag{1.2}$$

$$P = |\frac{1}{2\pi}\int_{-\infty}^{\infty} X(F)H(F)\mathrm{e}^{j2\pi Ft}dF|^2 \ . \tag{1.3}$$

where:

$y(t)$ = Filter Output (Time domain)

$X(F)$ = Frequency Domain input Signal

$H(F)$ = Frequency Domain Matched Filter

F = Frequency

t = Time

In order for the SNR to be increased, the noise power of the system should not increase after the influence of the filter. The noise power of the output of the filter can be estimated by first defining the power spectral density of the noise. Assuming the input noise into the filter has a power spectral density of $S_n(F)$, the power of the output noise can be estimated by integrating the power spectral density over all frequencies, as shown in equation (1.4). The output power can now be used with the result from equation (1.3) to find the SNR at the output of the matched filter, given the input signal x(t) and noise with a power spectral density of $S_n(F)$

$$P_n = \int_{-\infty}^{\infty} S_n(F)|H(F)|^2 dF \ . \tag{1.4}$$

Finally, defining SNR as the power of the signal P over P_n, and using equations 1.3 and 1.4, the SNR of the output of the matched filter can be represented as the

following:

$$\frac{P}{P_n} = \frac{|\frac{1}{2\pi}\int_{-\infty}^{\infty} X(F)H(F)\mathrm{e}^{j2\pi Ft}dF|^2}{\frac{1}{2\pi}\int_{-\infty}^{\infty} S_n(F)|H(F)|^2 dF} \quad . \tag{1.5}$$

In most applications, the noise of the system is considered to be both "white" and a stationary process. wide sense stationary, white noise has a uniform spectral density that is often represented as $\frac{N_0}{2}$, where N_0 is the input noise of a given unit bandwidth [2]. For white noise, the power of the output noise after the filter can be represented in the same way the signal power was estimated above. The output power spectral density becomes $\frac{N_0}{2}|H(F)|^2$. Substituting the white noise power spectral density into equation (1.4), the power calculation becomes the following:

$$P_n = \frac{1}{\frac{N_0}{2}2\pi}\int_{-\infty}^{\infty} |H(F)|^2 dF \quad . \tag{1.6}$$

Using equation (1.6) for the white noise case, equation (1.5), the SNR of the matched filter is estimated in equation (1.7):

$$\frac{P}{P_n} = \frac{|\frac{1}{2\pi}\int_{-\infty}^{\infty} X(F)H(F)\mathrm{e}^{j2\pi Ft}dF|^2}{\frac{1}{\frac{N_0}{2}2\pi}\int_{-\infty}^{\infty} |H(F)|^2 dF} \quad . \tag{1.7}$$

Since the goal is to maximize the SNR, further simplification of equation (1.7) can be done using the Schwarz inequality (equation (1.8)). Using the Schwarz inequality allows for the numerator and denominator of equation (1.7) to be separated. The $H(F)$ that will maximize the SNR can then be found:

$$|\int_{-\infty}^{\infty} X(\omega)Y(\omega)d\omega|^2 \leq \int_{-\infty}^{\infty} |X(\omega)d\omega|^2 \int_{-\infty}^{\infty} |Y(\omega)d\omega|^2 \quad . \tag{1.8}$$

After applying the Schwarz inequality with the interest of maximizing the SNR at a specific time T_p, equation (1.7) becomes equation (1.9):

$$\frac{|\frac{1}{2\pi}\int_{-\infty}^{\infty} X(F)H(F)\mathrm{e}^{j2\pi FT_p}dF|^2}{\frac{1}{\frac{N_0}{2}2\pi}\int_{-\infty}^{\infty}|H(F)|^2dF} \leq \frac{\frac{1}{2\pi}^2\int_{-\infty}^{\infty}|X(F)\mathrm{e}^{j2\pi FT_p}|^2dF\int_{-\infty}^{\infty}|H(F)|^2dF}{\frac{1}{\frac{N_0}{2}2\pi}\int_{-\infty}^{\infty}|H(F)|^2dF} \quad . \tag{1.9}$$

The Schwarz inequality is maximized when the two sides of the inequality are equal. Canceling common terms after applying the maximized Schwarz inequality yields equation (1.10):

$$\frac{P}{P_n} = \frac{2}{N_0 2\pi}\int_{-\infty}^{\infty}|X(F)\mathrm{e}^{j2\pi Ft}|^2dF \quad . \tag{1.10}$$

Closer inspection of equation (1.10) shows that the term $\frac{1}{2\pi}\int_{-\infty}^{\infty}|X(F)\mathrm{e}^{j2\pi FT_p}|^2dF$ looks very similar to the inverse Fourier transform shifted by T_p. However, the sign of the exponential is reversed. Thus, the inverse Fourier transform here becomes the conjugate of the signal x(t). Converting equation (1.10) back into the time domain, as shown in equation (1.11), shows that the SNR for a wide sense stationary, white noise signal is equal to the twice the power of the signal over the noise per unit bandwidth:

$$\begin{aligned}\frac{P}{P_n} &= \frac{2}{N_0 2\pi}\int_{-\infty}^{\infty}|X(F)\mathrm{e}^{j2\pi FT_p}|^2dF \\ &= \frac{2}{N_0}|x^*(T_p - t)|^2 \qquad (1.11) \\ &= \frac{2P}{N_0} \quad . \qquad (1.12)\end{aligned}$$

Note that the matched filter that maximizes SNR at a specific time T_p becomes the time reversed conjugate of the original signal. The matched filter for a signal with

an arbitrary amplitude A can be expressed as shown in equation (1.13):

$$h(t) = Ax^*(T_p - t) \ . \tag{1.13}$$

As a result, modulated complex base band signals are conjugated and time reversed in the construction of the matched filter. In addition, an example of the real components of a matched filter for a linear frequency modulated signal is shown in Figure 1.2.

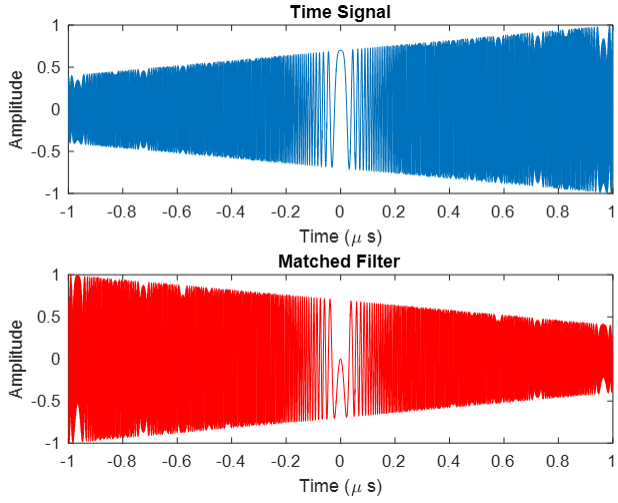

Figure 1.2: Matched Filter Linear Frequency Modulated Signal

For example, consider a system that utilizes a linear frequency modulated signal and has a stationary target reflecting the waveform back. The SNR of the received waveform can be increased by convolving it with the time reversed conjugate of the signal. An example of how the matched filter works is shown in Figure 1.3. The idea is that when the time reversed signal is put into the convolution integral, the time reversed signal is "flipped" and the convolution integral becomes a cross-correlation integral:

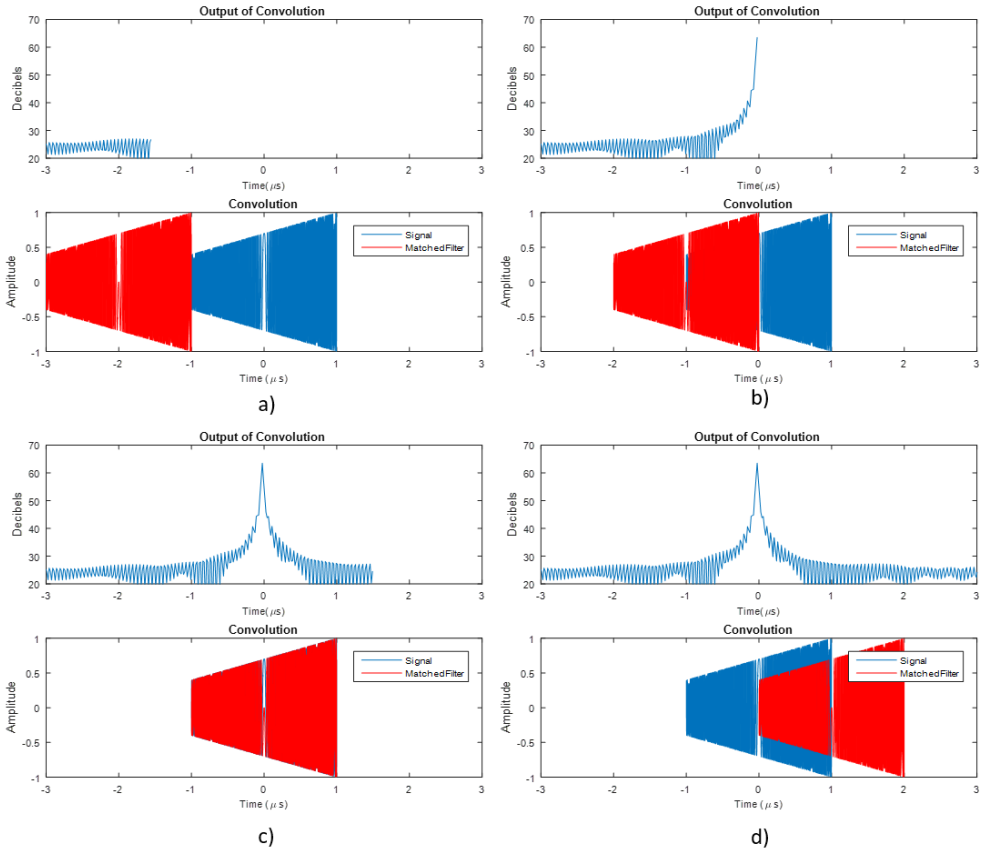

Figure 1.3: Steps of the Matched Filter Convolution

$$y(t) = \int_{-\infty}^{\infty} x(\tau)h(t-\tau)\delta\tau \quad . \tag{1.14}$$

For example, in equation (1.14), if the signal x(t) is the time reversed conjugate, the equation becomes equation (1.15):

$$y(t) = \int_{-\infty}^{\infty} x^*(-\tau)h(t-\tau)\delta\tau \quad . \tag{1.15}$$

Further manipulation of equation (1.15) can be done by letting τ' be the $-\tau$ variable and adjusting the integration variable to be $-\delta\tau'$. After this substitution, equation

(1.16) is obtained:

$$y(t) = \int_{-\infty}^{\infty} x^*(\tau')h(t+\tau')(\delta\tau) \ . \tag{1.16}$$

Equation (1.16) is the equation used for calculating the cross correlation of two signals. Given the matched filter to be $x(t)$ and the received signal as $h(t)$, the same process can be used to perform the matched filter algorithm. Computationally, using cross correlation is slightly more efficient, since the signal used for the matched filter is manipulated less. For example, using the convolution technique requires the signal used to be conjugated and time reversed. Then, when performing the convolution the signal is time reversed once more and multiplied by the received signal. Whereas the cross correlation technique only requires the signal to be conjugated and multiplied by the received signal.

The scope of this thesis deals explicitly with amplitude distortions created by digital electronics in digital radar systems. The waveform tested was a linear frequency modulated signal, described in chapter 2, that is popularly used in radar systems. The designed and tested predistortion method, described in chapter 3, mitigates the distortions and generates a more ideal waveform transmitted by the radar. The method proposed was tested on two separate systems, described in chapter 4, and proved successful in producing a more ideal waveform with significantly less distortions. The predistortion method created a waveform with a more flat envelope on the output of the transmitter. The resulting signal more closely matches the ideal waveform used when implementing pulse compression. The designed method produces a waveform with a lower amplitude compared to the ideal waveform. It was found that the predistortion technique produced an improvement in the output of the matched filter despite the lower amplitude waveform. The technique was also implemented in a basic radar system and was successful in producing improved results, detailed in chapter 5. In addition, the method was tested with

different bandwidths described in chapter 6. The method also proved successful with the inclusion of amplifiers described in chapter 7. Lastly, chapter 8 shows some results gathered from data collected from the fielded radar. The technique designed and tested in this thesis successfully mitigates the distortions caused by digital components. The method becomes attractive for multiple channel systems that utilize individual excitation circuits for each channel. The technique can be utilized to allow these systems to more reliable transmit the same waveform across all the channels. In systems that utilize beam forming, the technique also allows for algorithms to more reliably transmit the desired beam, as detailed in chapter 9 and 10.

2 Waveforms

Traditionally, radar waveforms continuously propagate a signal with a ramp-like modulated frequency. The received waveform is then converted to frequency and plotted against time. The range can then be extracted by the time delay between frequency patterns. Modern radar waveforms are often transmitted in pulses to maximize the signal to noise ratio when receiving. The idea is to transmit the waveform for as long as possible before the front of the reflected waveform reaches the radar receiver. This allows the system to transmit as much signal as possible to increase signal to noise. However, transmitting while the radar is receiving is impossible while using one antenna. When using multiple antennas, mutual coupling occurs if the radar is receiving while transmitting. Pulsing the waveform allows for the mutual coupling between the antennas to be removed. While the system is receiving the reflected wave, the transmitting wave is turned off. This removes the cause of the mutual coupling. Furthermore, pulsing the waveform allows for a radar to use only one antenna to both transmit and receive the waveform. In order to use one antenna to both transmit and receive, the system is configured to begin receiving in between transmitted pulses. For example, when the transmitted pulse ends, the antenna begins to receive the waveform reflected from the closest target of interest. The range can then be extracted by measuring the time between the end of the transmitted pulse to when the pulse is received. The waveform chosen for the radar is a pulsed linear frequency modulated (LFM) signal, often called a chirp, shown in Figure 2.1.

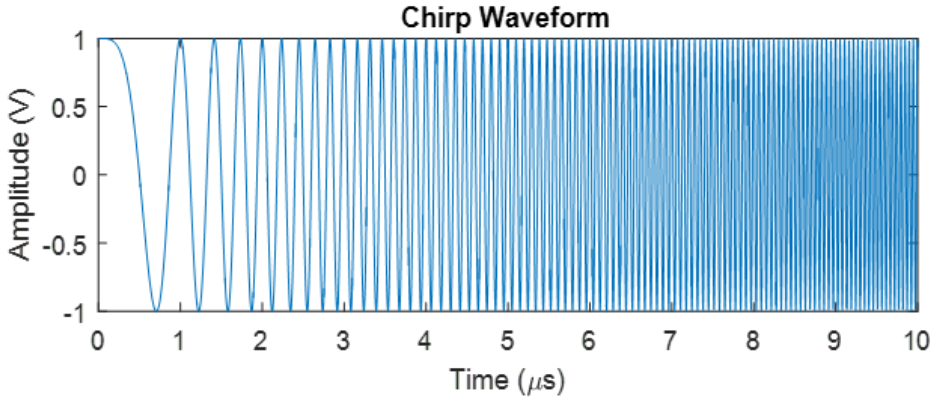

Figure 2.1: A Linear Frequency Modulated Signal (Chirp)

LFM waveforms are signals that span a predetermined bandwidth. The frequency of the waveform changes in an exponential pattern. LFM waveforms are classified into two categories. These two categories are an up chirp, which increases with time, or down chirp, which decreases with time. LFM waveforms for the desired application were created using the following equation, with the frequency starting at the lower limit and increasing to the upper limit (up chirp):

$$a(t) = A\mathrm{e}^{j\pi\beta Tt^2} \quad . \tag{2.1}$$

Where:

$A =$ Amplitude

$\beta =$ Bandwidth

$T =$ Pulse Width

$t \ =$ Time

The disadvantage to pulsed waveforms is a concept called *blind range*. Blind range is the range associated with the time lost when the radar is transmitting. Ideally, the blind range of a radar is chosen in the design of the waveforms, and can

be configured to the radar application. The blind range is constrained by the range to the first target of interest. The range to the target is calculated by the time the transmitted waveform takes to reflect off the target and return to the radar traveling at the speed of light. For instance, a short range radar having a pulse width of 1 μs results in 150 meters of blind range. This means anything short of 150 meters is essentially "blind", or undetectable to the radar. Equation (2.2) shows how range is calculated given a specified time and transition time, t, defined as the non-ideal amount of time required by electronics. In most applications, the transition time can be assumed to be zero. As found by [11], the transition time in most electronics were on the order of picoseconds

$$R = \frac{c(\tau + t)}{2} \quad . \tag{2.2}$$

Where:

c = Speed of light

τ = Specified Time

t = Transition Time

R = Blind Distance

The bandwidth of a non-modulated signal is equivalent to the inverse of the waveform pulsewidth. The use of modulated waveforms allows for the concept of *pulse compression*. The process of pulse compression involves the utilization of the matched filter. Instead of increasing pulse length to achieve better signal-to-noise, the bandwidth is increased via modulation, and the pulsewidth transmitted is minimized. Equation (2.3) is used in calculating range resolution given a bandwidth:

$$\Delta R = \frac{c}{2\beta} \quad . \tag{2.3}$$

Where:

c = Speed of light

β = Bandwidth

ΔR = Range Resolution

Thus, modulating a waveform only becomes effective if the bandwidth is much larger than the bandwidth of a non-modulated, simple pulse, $1/\tau$. The goal is to maximize the bandwidth in each transmitted pulse in order to minimize the spacing in the range bins, or range resolution, observed by the system. A range bin is a set of values that are used to classify the range of the received target based off of the time delay received. In other words, a range bin takes any distance within the range of values and maps the range of the target to the single value. For example, if a target is detected at 10.5 meters, but the range bin is set to have any values between 10-12 meters be mapped to 11 meters, the detected target range becomes 11 meters. In addition, radar systems usually use multiple range bins that are spaced evenly apart. The spacing between range bins is simply the width of the range bins. In the previous example, the range bin spacing is two meters. This means every two meters gets mapped to a single meter. By decreasing the spacing in range bins, more fine tuned range sampling is achieved, which translates to higher range resolution. For instance, if the range spacing is half a meter, then the radar can detect targets separated by half a meter.

Coherent radars allow for the detection of phase changes. This is because the waveforms have a phase reference between each pulse. Waveforms with real components can only detect a phase change in one direction. For instance, when a radar wave reflects off a target moving toward the radar a positive phase change is induced. The radar then detects the phase change between the previous pulse and the latest received to determine if the target is moving toward the radar. However, when a radar wave is reflected off a target that is moving away from the radar, a negative

phase change is induced. The negative change in phase is an imaginary component, meaning a real valued signal will alias the negative change to a positive change. As a result, radar waveforms utilizing real values cannot differentiate between targets moving away from the radar and targets moving toward the radar.

2.1 Ambiguity Function

The matched filter becomes ideal for stationary targets where no changes are inflicted on the waveform that is reflected back. However, in practical applications distortions are caused by a number of items. The most common type of distortion is if the target is not stationary when the waveform is reflected back. The motion of the target introduces a distortion that slightly alters the frequency of the waveform. The shift in frequency is referred to as the Doppler shift. For the concept of the matched filter to be optimized, the waveform used for the matched filter must "match" the received waveform as much as possible. In general, the more the signal is matched, the more SNR will increase. The introduction of Doppler shift into the received waveform implies the received waveform no longer matches the waveform used for the matched filter. The response of the matched filter then changes and produces a slightly different SNR for the received waveform.

For SAR applications, it is fundamental to have movement of the radar with respect to the target in order to form an image. In some cases, the target and the radar are both moving, and each introduce Doppler shifts into the waveform. In addition, some SAR systems are mounted on high speed vehicles, such as airplanes. The amount of Doppler shift introduced by a target increases as the speed between the radar and the target increases. This means the waveform must be able to support the amount of Doppler shift induced by the motion of both the radar system and the targets of interest.

A common tool utilized in waveform design is the ambiguity function. The ambiguity function is a three dimentional plot that shows the output of the matched filter for various time delays and Doppler shifts for noiseless reflected waveforms [12]. The ambiguity function can be used to determine if the expected amount of Doppler shift induced by the target can be represented by the designed waveform. The ambiguity function also shows the amount of ambiguity in target detection. The ambiguity function becomes particularly useful when observing the amount of attenuation of the output of the matched filter at each time delay and Doppler shift.

The ambiguity function can be calculated by using a time signal with an arbitrary Doppler shift F_d. The signal in the time domain can be represented by equation (2.4):

$$x(t) = \cos(2\pi F_0 t + 2\pi F_d t) + j\sin(2\pi F_0 t + 2\pi F_d t) \ . \tag{2.4}$$

In equation (2.4), F_0 is the center frequency of the waveform. Taking into consideration that the transmitted waveform, x_{in}, contains no Doppler shifts, the transmitted signal can be represented as equation (2.5) with the help of the Euler identity:

$$x_{in}(t) = \cos(2\pi F_0 t) + j\sin(2\pi F_0 t) = \mathrm{e}^{j(2\pi F_0 t)} \ . \tag{2.5}$$

Equation (2.4) can then be combined with equation (2.5) to produce an exponential form of the reflected waveform from a moving target, shown in equation (2.6):

$$x(t) = x_{in}(t)\mathrm{e}^{j(2\pi F_d t)} \ . \tag{2.6}$$

With a matched filter created to match the signal in equation (2.5), the signal in equation (2.6) will be placed in the convolution integral with the matched filter.

The convolution integral becomes equation (2.7):

$$A(t, F_d) = \int_{-\infty}^{\infty} x_{in}(\tau) \mathrm{e}^{j(2\pi F_d t)} x_{in}^*(t-\tau)\delta\tau \quad . \tag{2.7}$$

Equation (2.7) is the mathematical representation of the ambiguity function. The ambiguity function is a function of the time delays, t, and the Doppler shifts introduced by a moving target, F_d. The actual ambiguity diagram is created by varying both variables and creating a three-dimensional plot. The matched filter can be created to match the transmitted waveform with zero Doppler shift, and a time delay that corresponds to a point in the middle of the radar range scene. In other words, the ideal matched filter is calculated to be matched to a stationary target in the middle of the target area. The matched filter can then be applied to the received waveform with varying Doppler shifts for every time delay. The results of each Doppler shift and time delay can be represented graphically. The varying Doppler shifts are placed on one axis, and the varying time is placed on another axis. Lastly, the amplitude output of the matched filter is placed on the third axis. The three dimensional plot shows the amount of attenuation as the waveform becomes more and more mismatched from the matched filter. In addition, the ambiguity function also displays the expected response of the matched filter given a specific time delay and Doppler mismatch. For a simple pulse, shown in Figure 2.2, the ambiguity function will show how the pulse responds to varying time delays and Doppler shifts.

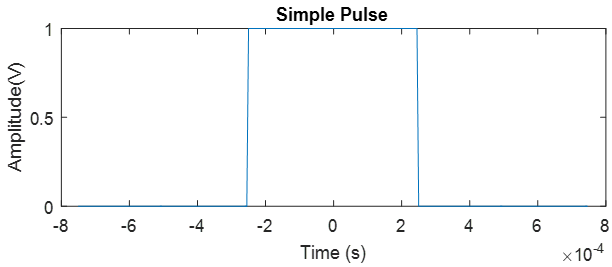

Figure 2.2: Simple Pulse

For the simple pulse shown in Figure 2.2, it makes sense that as the frequency becomes more mismatched, the output diminishes quickly. This is because the simple pulse can not detect frequency shifts. For instance, the simple pulse contains no frequency, which is reflected in the ambiguity function as not being able to detect a Doppler shift. For the simple pulse waveform, the output of the matched filter gradually decreases as the time delays deviate from the matched time. For instance, the simple pulse is a real valued rectangle pulse, meaning the output of the matched filter is the same as the convolution of two rectangle pulses. Since the waveform is a simple pulse, as the time is more mismatched, the amount of overlap in the convolution integration is less. This, in turn, yields a lower returned power. As a result, the ambiguity function, shown in Figure 2.3, can be created for a simple pulse.

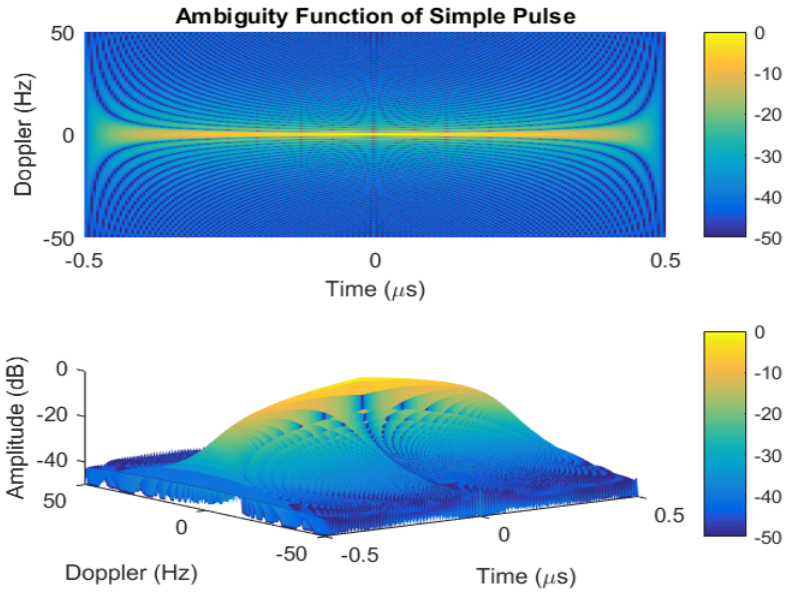

Figure 2.3: Ambiguity Function of a Simple Pulse

The output amplitude of the ambiguity function of a simple pulse diminishes quickly as the Doppler shift deviates from the matched Doppler. The effects of Doppler shifts and time delays on returned power become obvious when viewing the zero Doppler and zero time delay cuts of the ambiguity function. The zero Doppler and time delay cuts are shown in Figure 2.4. Notice, as the time delays are varied with no Doppler shift, the output of the matched filter has a pretty large response. This means the resolution of the targets at different ranges is ambiguous. In other words, two targets that are at distances that produce time delays within the width of the zero Doppler cut response appear as one target to the radar.

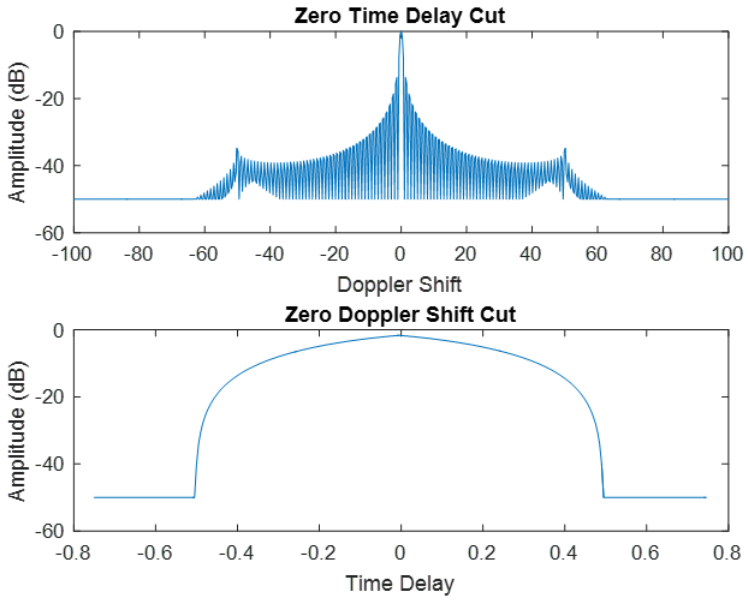

Figure 2.4: Zero Doppler and Time Delay Cuts of the Ambiguity Function

On the other hand, the resolution in the Doppler shifts for a simple pulse is great, since the width of the zero time Delay cut is small. Different waveforms produce different ambiguity functions, and each waveform has different qualities that make them unique. For example, a chirp waveform is more tolerant to Doppler shifts and time mismatches [12]. For the chirp shown in Figure 2.5, the ambiguity function illustrates the tolerances, showing the range of Doppler shifts that can be represented.

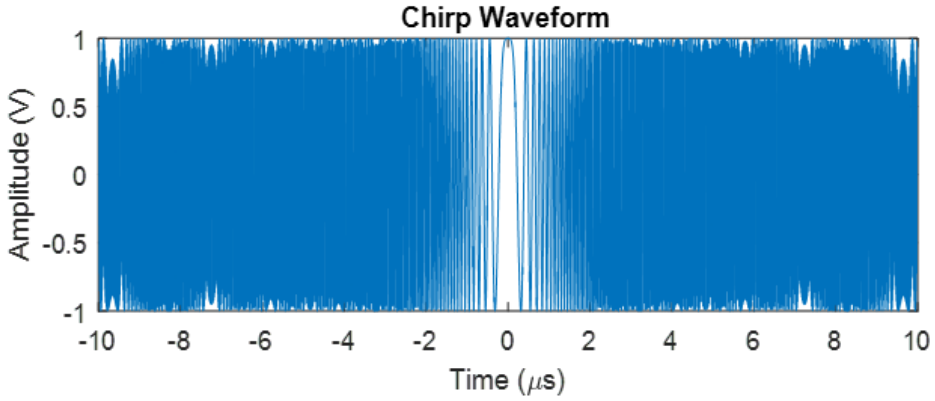

Figure 2.5: Chirp Pulse

As seen in Figure 2.6, the attenuation of the matched filter tapers off significantly slower as the time delays become more and more mismatched. In addition, the amount of Doppler shift and time delays that can be represented is significantly more than the simple pulse.

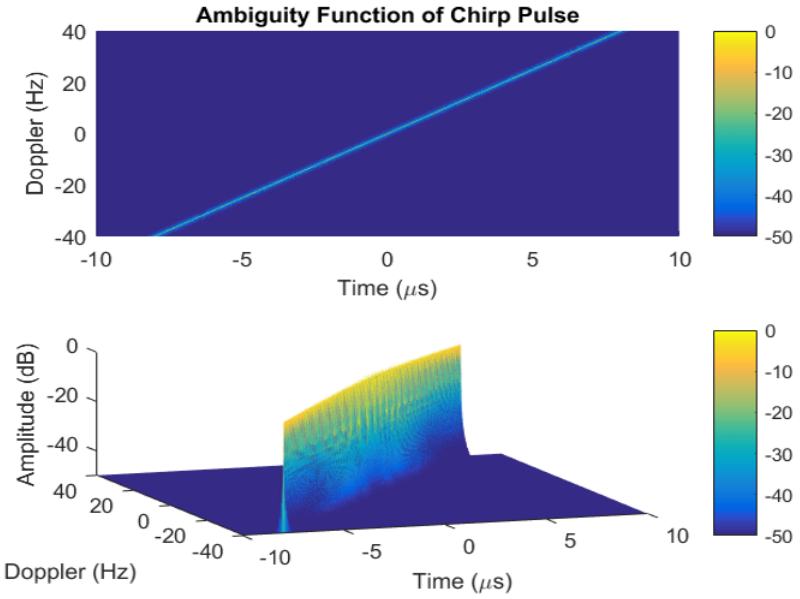

Figure 2.6: Ambiguity Function of a Chirp Pulse

Furthermore, Figure 2.7 show the zero Doppler and time delay cuts for a chirp waveform. As seen in Figure 2.7, the resolution in both Doppler and time delays are significantly better than that of the simple pulse shown previously. The relative side lobes of each cut are also significantly lower than the main peak of the matched filter response. This means the response of the matched filter can more accurately represent the detection of a reflected wave. In addition, the matched filter can more accurately represent range and the speed of the target because the response of the matched filter is very small in both cuts.

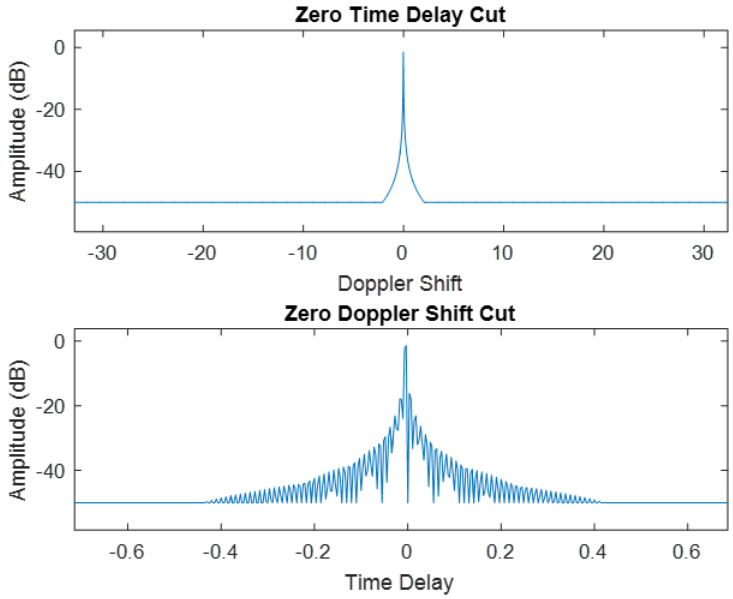

Figure 2.7: Zero Doppler and Time Delay Cuts of Ambiguity Function of a Chirp Pulse

2.2 Under Sampling

The concept of under sampling, also known as band pass sampling, allows analog to digital converters (ADCs) to sample higher frequency signals at a lower speed. Normally, ADCs are forced by the Nyquist sampling theorem to sample

at twice the maximum frequency in order to prevent aliasing and signal distortion. For example, if a regular sinusoidal signal with a frequency of 100 MHz was sampled at 100 MHz, the sampled signal would actually appear as a constant. Sampling a signal at its own frequency translates to taking one sample per period of the signal, which means that the same point is sampled every cycle. The ADC interprets this phenomenon as a constant voltage. Conversely, sampling at twice the carrier frequency translates to sampling twice per period. For a sinusoidal signal, sampling twice per period will sample both the minimum and the maximum of the sinusoid. This allows for the system to create a signal at the same frequency.By definition, bandpass sampling is a special form of undersampling that translates a high-frequency bandpass signal to a baseband frequency [13–20]. This concept provides a technique of reduced sampling speeds, which directly translates to reduced power consumption (as the authors have been able to demonstrate in [21][22]).

Furthermore, when the signal is sampled at half the frequency, the signal returned will be half the frequency desired. Sampling at half the signal frequency translates to taking a sample point every other period. The first sample will be a minimum and the second sample will be a maximum of the signal, causing the returned signal to be half the frequency. In radar systems, the frequency on the received waveform side is not actually relevant, since the range and motion of the target is derived from the timing and phase of the received waveform. For this reason, under sampling becomes attractive because sampling at a lower frequency also reduces the amount of data collected by the radar, while still preserving the data required to extract the range and the motion of the target. The concepts of Nyquist zones and the Nyquist-Shannon sampling theorem allow for the required data to be preserved. Nyquist zones are the regions in the frequency domain where a sampled signal can be represented while preserving data. By the Nyquist-Shannon sampling

theorem, a signal in the higher Nyquist zones can only be reconstructed in the first zone if the signal is sampled at a minimum of twice the bandwidth of the signal of interest. As long as the Nyquist-Shannon theorem is satisfied, the aliased image shown in Figure 2.8 can completely represent the actual signal at a lower frequency.

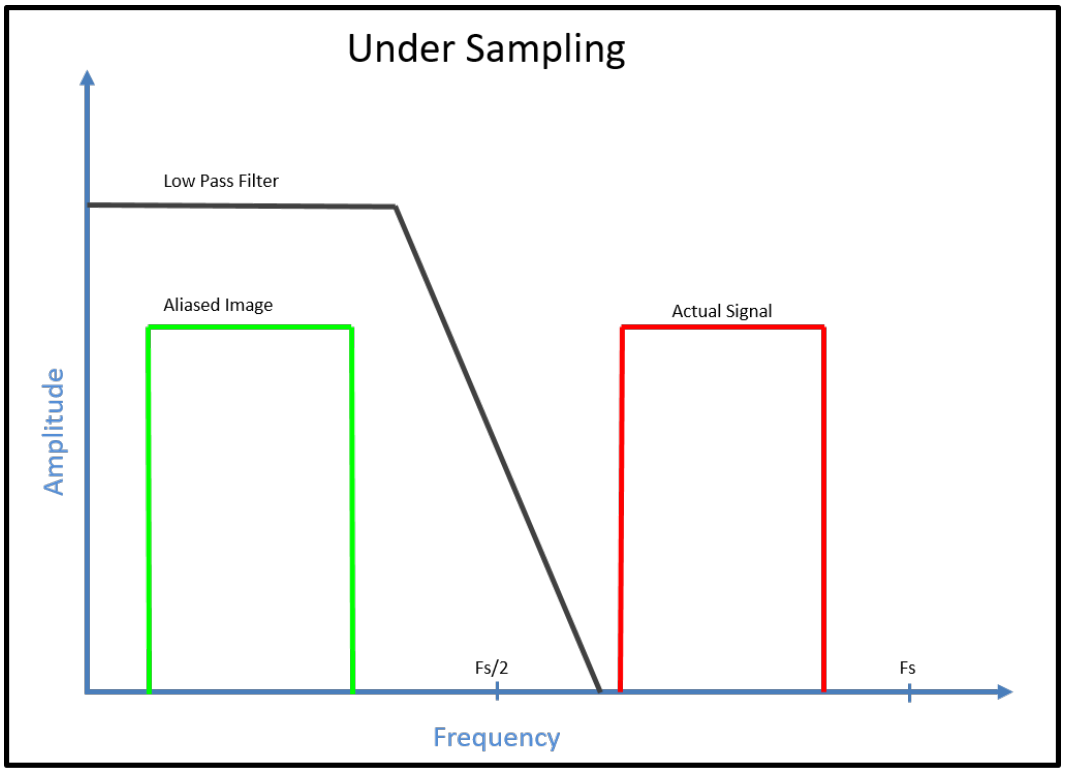

Figure 2.8: Visualization of Under Sampling

Figure 2.8 shows the actual signal in the region defined as the second Nyquist zone. In addition, the aliased image is represented in the region defined as the first Nyquist zone. For the application described in chapter 3, the signal of interest is sampled in the manor shown in Figure 2.8. Figure 8 in [23] illustrates the phenomenon of Nyquist zones in more detail. However, ADCs are limited by Nyquist in how they represent signals, because most ADCs are designed to sample at twice the desired frequency. If an ADC is sampling at a sampling frequency, f_s, the max-

imum signal that can be represented by the ADC is $f_s/2$. For instance, if a signal is centered at 400 MHz and is sampled at 180 MHz, then the signal returned will be centered at 220 MHz. This signal cannot be represented by the ADC because Nyquist states that the max value the ADC can represent is 90 MHz. Therefore, it is crucial that the sampling rate for the ADC be chosen such that the difference between the maximum desired frequency and the sampling frequency is less than half of the sampling frequency. For a chirp waveform or a waveform with a bandwidth, it is important that the under sampling rate does not alias any part of the waveform, since the bandwidth is directly related to the range resolution of the radar. For instance, a chirp with a bandwidth of 200 MHz centered around 435 MHz cannot be under sampled by half the carrier frequency (217.5 MHz). If the 200 MHz chirp is sampled at 217.5 MHz, the signal will be centered around 217.5 MHz. According to Nyquist, half the waveform will only be represented at $f_s/2$. As a result, half the waveform is received on the left side of 108.25 MHz. In order to represent the waveform completely, the difference between sampling frequency and the bandwidth must be greater than the half the bandwidth. For the 200 MHz bandwidth signal centered at 435 MHz, a valid sampling frequency can be 600 MHz. Sampling at 600 MHz will alias the signal down to 135 MHz, and the maximum the signal can be represented by sampling at 600 MHz is 300 MHz. With the signal aliased down to 135 MHz, the upper and lower bounds of the signal is 235 MHz and 35 MHz, respectively. The undersampling technique is utilized commonly in digital radar systems [24] and has worked in the past [21].

3 Predistortion

The concept of predistortion is to distort the original signal in such a way that the distortions are reversed by the system to produce the desired output. As described in [25], noise and distortion can be differentiated because distortion is a fixed effect on the signal, where as noise is a statistically random process. The distortion defined as the system response can be compensated for by "predistorting" the waveform before it is influenced by the system. For instance, when implementing linear frequency modulated (LFM) waveforms in hardware for radar transmission, the hardware induces an amplitude modulation. The amplitude modulations are caused by the hardware being incapable of creating sharp, rapid changes in voltage. The amplitude modulation can be referred to as the system response and is shown in Figure 3.1.

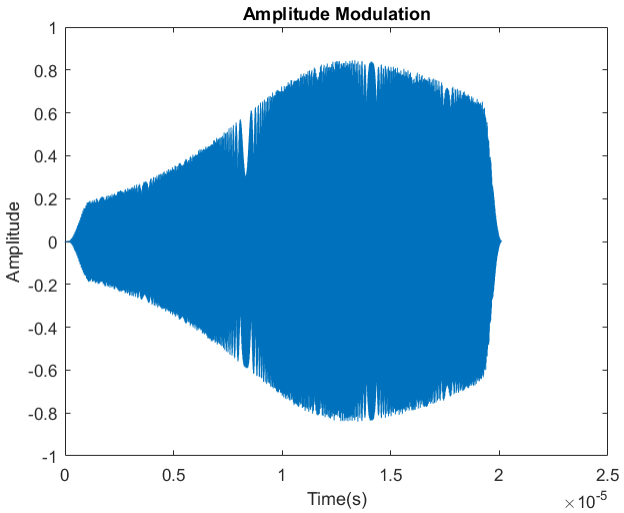

Figure 3.1: An Example of Amplitude Modulation

The system response causes the LFM to not have constant power over the radar pulse, which then affects the range of the radar over the pulse. To maximize the range detection of the radar, the maximum power transmitted for a LFM pulse

should have a constant modulus. Ideally, this should be at the maximum voltage of the waveform. In order to achieve a constant modulus, the system response must be removed. The technique used to removed the system response starts with the input waveform being predistorted by the opposite of the system response. This means that when influenced by the system a constant modulus waveform is produced. The predistortion technique used requires the system response to be only a distortion in amplitude and not contain a distortion in phase. In addition, the concept of predistortion requires the system response must be deterministic, meaning the system response does not change from pulse to pulse. The technique used is applied in the calibration stage of the radar. Thus, the technique will be applied once every time the system is powered on, and the predistortion calculated will be applied to all pulses in that data collection period. If the system response is not deterministic, the predistortion will not be applicable for every pulse. In addition, due to the way the predistortion is calculated, the system response would have changed by the time the system applied the calculated predistortion if the system response is not deterministic. As for phase, the technique used is designed to remove amplitude distortions and does not affect phase, whether the phase is distorted or not. If the system response introduces unwanted phase, then the proposed technique will not remove the undesired phase.

However, the response will vary from system to system, and any components added or removed from the system will create a different system response. Furthermore, the response can even change from system run to system run. For example, simply power cycling the system could cause it to produce a slightly different system response. The technique proposed must be applied again for each run to acquire a new predistortion capable of correcting the new changes in the system. If the system response is only in amplitude and is deterministic, then the predistortion

applied to the input waveform can be characterized as the inverse of the system response envelope. Mathematically, the amplitude distortion is a constant influencing the waveform with time varying phase $\theta(t)$, as shown in (3.1). Since the amplitude modulation can be characterized as a time varying component $a(t)$, the effects of the component can easily be removed by doing the inverse operation shown in (3.2)

$$x(\mathrm{e}^{j\theta(t)}) = a(t)\mathrm{e}^{j\theta(t)} \tag{3.1}$$

$$x_{des}(\mathrm{e}^{j\theta(t)}) = \frac{1}{a(t)}x(\mathrm{e}^{j\theta(t)}) \tag{3.2}$$

where $x(\mathrm{e}^{j\theta(t)})$ is the signal with amplitude distortion and $x_{des}(\mathrm{e}^{j\theta(t)})$ is defined as the desired signal. Predistorting the input signal with the inverse of the system response envelope, requires the system response to be obtained and finding the effects of the system on the input reference waveform after the system. The effects of the system on the input signal can only be obtained by sending the a reference LFM signal through the system and observing the differences between the received signal distorted by the system and the input reference signal. The distorted waveform is used to estimate the amplitude distortion provided by the system response. Assuming the distortion from the system contains only amplitude distortions, the distortion can be modeled by the envelope of the signal. The envelope is then inversed and multiplied by the reference waveform to obtain the predistorted waveform. The predistorted waveform is then re-transmitted and acquired via the Analog to Digital Converter (ADC). The resulting signal should have significantly less amplitude modulation if any at all. In addition, the signal should have a smaller power level as the predistortion technique does not create a constant modulus at the maximum amplitude of the signal. The technique creates a constant modulus signal at the average amplitude of the envelope portraying the system response.

3.1 Phase Distortion

In order for the predistortion technique to work the signal must not contain any distortions in phase. Distortions in phase cause irregularities in amplitude that can not be detected via envelope estimation. For instance, a phase distortion of 180 degrees for example, can cause a drastic trough in the signal modulus. In addition, phase distortions could be undeterministic where the phase could be distorted at the beginning of the waveform and as the system is being exercised the phase distortion begins to walk across the waveform. The predistortion technique requires the envelope estimation to be a smooth estimation of the signal modulus in order to guarantee the inverse of the modulus is defined. For instance, waveforms with phase distortions can cause the signal modulus to drop near zero which becomes large with inverted meaning the modulus has the possibility of becoming undefined. The phase of the waveform is displayed in Figure 3.2 at each stage of the predistortion technique.

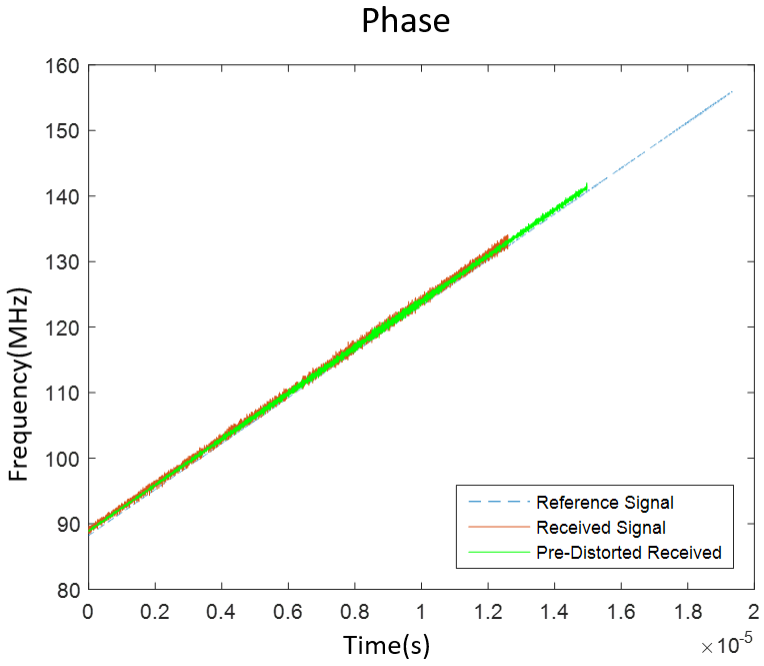

Figure 3.2: Phase of the Signal at Each Stage of Predistortion

It is shown that the frequency is consistent at each stage of the technique from the non predistorted waveform to the predistorted waveform. The phase of the signal is also consistent and shows that the system does not introduce a phase distortion that cannot be reversed by amplitude predistorting. In addition, Figure 3.3 shows a closer look in the frequency domain of the envelope of the waveform at each stage of the predistortion with the final picture being the predistorted envelope of the waveform after it has been influence by the system response. In addition, the predistorted waveform is an inverse of the estimated envelope for the received signal. As a result, the modulus of the waveform becomes more flat and contains less amplitude distortions.

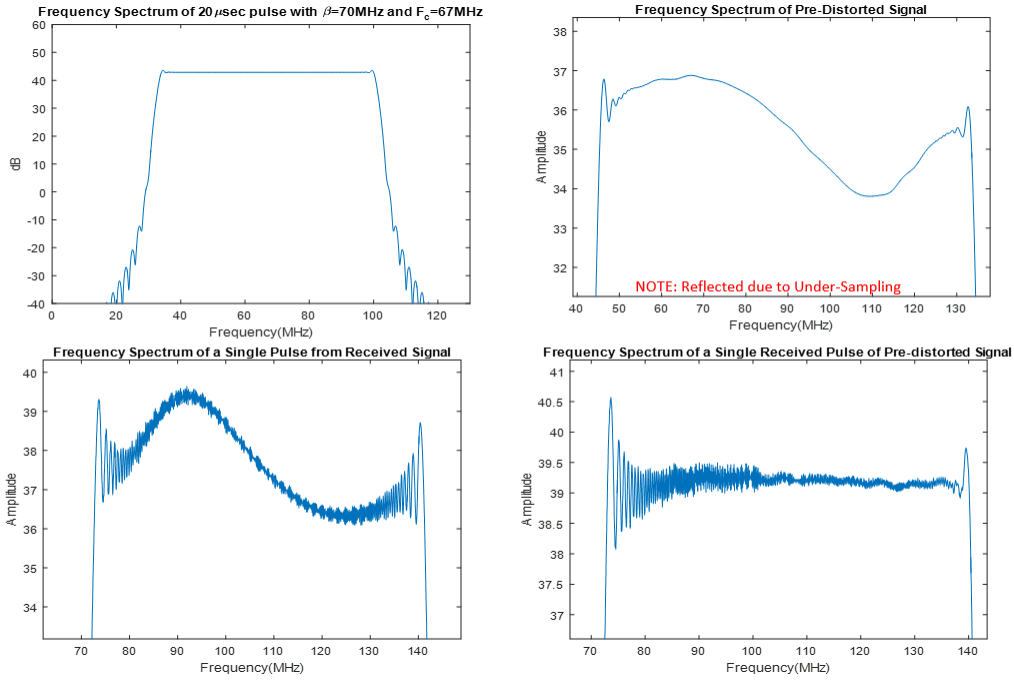

Figure 3.3: Envelope of the Signal at Each Stage of Predistortion

3.2 Envelope Estimation

The envelope of the received signal was estimated using MATLAB®'s envelope function. The function has three different methods of estimating the envelope of the signal. The first is the analytic method which returns the analytic envelope calculated by the Hilbert transform. The second method is rms where the envelope is estimated with the Hilbert transform and a moving rms filter. This method produces the envelope at the rms voltage of the signal. The last method is the peaks method which uses the Hilbert transform to derive an estimation of the envelope of the signal. The Hilbert transform is shown in equation (3.4) and equation (3.3) [26]. In the MATLAB® algorithm, the equation (3.3) is used to produce the real, or positive frequency, signal. The algorithm uses the Hilbert transform to calculate the analytic signal and then takes the absolute value to obtain only the positive

envelope. Finally, the function passes the envelope through a smoothing filter that removes the ringing in the envelope. The final product becomes a vector of values that outline the modulus of the input waveform when plotted:

$$X_{re}(e^{jw}) = \frac{1}{2\pi}\int_{-\pi}^{\pi} X_{im}(e^{jv})cot(\frac{w-v}{2})dv + x[0] \tag{3.3}$$

$$X_{im}(e^{jw}) = -\frac{1}{2\pi}\int_{-\pi}^{\pi} X_{re}(e^{jv})cot(\frac{w-v}{2})dv \ . \tag{3.4}$$

Where:

v = Phase(2 π frequency)

w = Phase(2 π frequency) transformed

X_{im} = Imaginary part of signal

X_{re} = Real part of signal

$x[0]$ = Frequency offset

To simplify, the envelope is estimated by taking the magnitude of the complex waveform and applying a smoothing median filter. The complex waveform is acquired by removing the negative frequency image then applying the magnitude of the remaining signal. The envelope is then smoothed by applying a smoothing median filter. The smoothing median filter can be configured to have more or less taps to control how "tight" the envelope estimation is. For instance, a median filter with a lesser amount of taps will produce an envelope that is closer to the absolute value of the analytic signal compared to a filter with more taps creates an envelope that will go from peak to peak in a sinusoidal signal producing an envelope estimation without the oscillations. The result is an envelope that more accurately captures the system response and not the values of the waveform. Each method analyzed for the predistortion technique is shown in Figure 3.4.

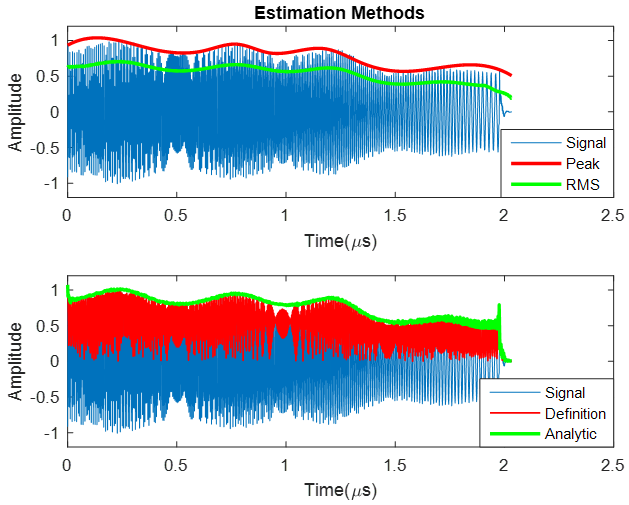

Figure 3.4: Envelope Estimation

In the Figure 3.4, the definition was calculated by using a simple definition of an envelope. The definition took the square root of the sum of the real component squared and the imaginary component squared, $\sqrt{R_e(x(t))^2 + I_m(x(t))^2}$. The definition did not outline the system response well. The result contained multiple oscillations and the system response is not visible. The RMS method captured the system response well but was not at the maximum amplitude. This means the envelope did not capture the max amplitude of the amplitude distortions. The analytic method outlined the system response nicely, however, the estimated envelope still contained a small amount oscillations. It was desired to apply a smooth predistortion in order to eliminate the chance of any undesired irregularities in the predistorted signal. An example of the effects of a smoothing filter are shown in Figure 3.5.

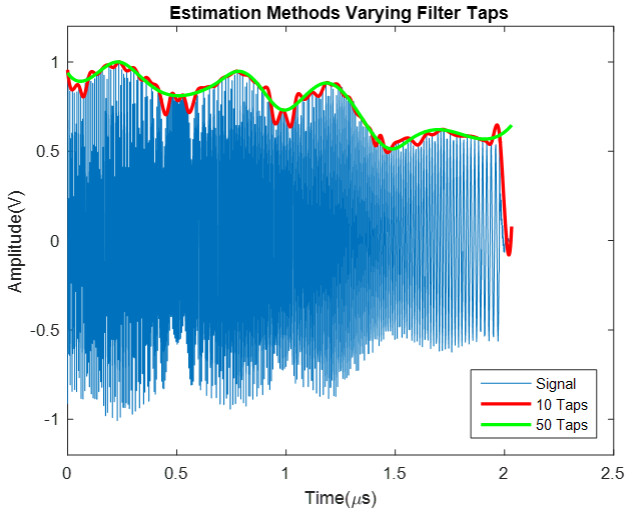

Figure 3.5: Effects of Filter Taps

The filter applied to the estimation method allows for the estimated envelope to capture the distortions caused by the system rather than the amplitude of the signal. In this application, the envelope is not the traditional envelope of the signal but rather the gradual amplitude distortions caused by the system. In the end, the peak method was determined to capture the system response the best and was utilized for the designed implementation. The received signal and the estimated envelope utilized with the smoothing filter applied is shown in Figure 3.6.

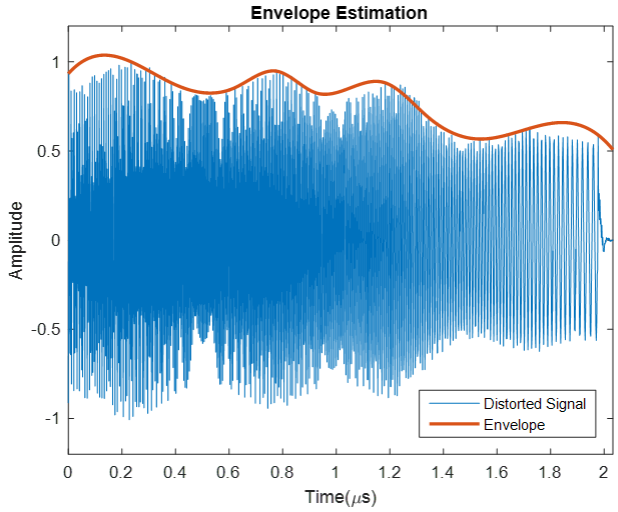

Figure 3.6: Envelope Estimation

The estimated envelope is now defined as the system response and the predistortion needed to reverse the effects cause by the system is simply the inverse of the system response. The waveform initially transmitted is then multiplied by the predistortion. A Tukey window was utilized to minimize any overshoots the system might induce due to the beginnings and ends of the waveform. The Tukey window also compensates for the bounds of the predistotion envelope. The equation for a Tukey window is shown in (3.5) [27][28]. In equation (3.5), the variable r is the ratio of the window that is non constant. The Tukey window was chosen because of the amount of control over the unity pass band of the signal. A graphical example of some Tukey windows are shown in Figure 3.7. Note the window becomes the familiar cosine window when $r = 1$. The Tukey window removes the overshoot

and provides a significantly smoother transition for the DAC to synthesize

$$T(x) = \begin{cases} \frac{1}{2}[1 + cos(\frac{2\pi}{r}(x - \frac{r}{2})] & 0 \leq x < \frac{r}{2} \\ 1 & \frac{r}{2} \leq x < 1 - \frac{r}{2} \\ \frac{1}{2}[1 + cos(\frac{2\pi}{r}(x - 1 + \frac{r}{2})] & 1 - \frac{r}{2} \leq x \leq \frac{r}{2} \end{cases} . \tag{3.5}$$

Since the predistortion envelope is the inverse of the system response, The envelope can potentially be quite large since the waveforms are small (near zero) at the beginning and end of the pulse. Taking the inverse of a positive number near zero causes the predistortion envelope to potentially become undefined.

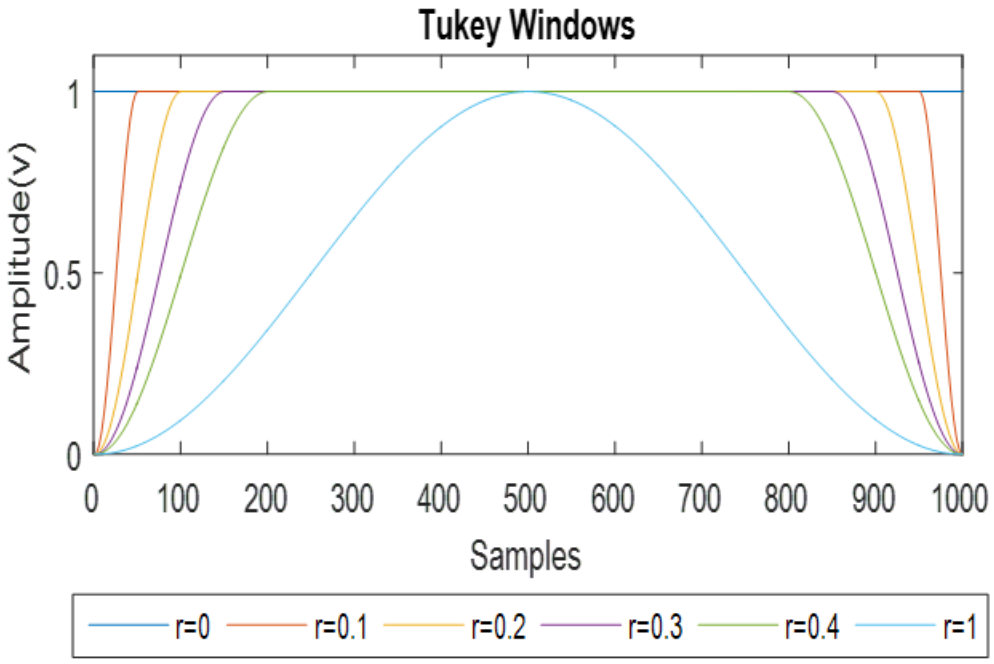

Figure 3.7: Tukey Windows

Since the undefined points are at the beginning and end of the waveform a Tukey window counteracts the undefined portion of the predistortion envelope. In the sys-

tem used, the Tukey window was set to have a length equal to the chirp waveform. In addition, the ratio of the waveform that was non constant was chosen to be $r = 0.1$. An example of the effects of the Tukey window is shown in Figure 3.8.

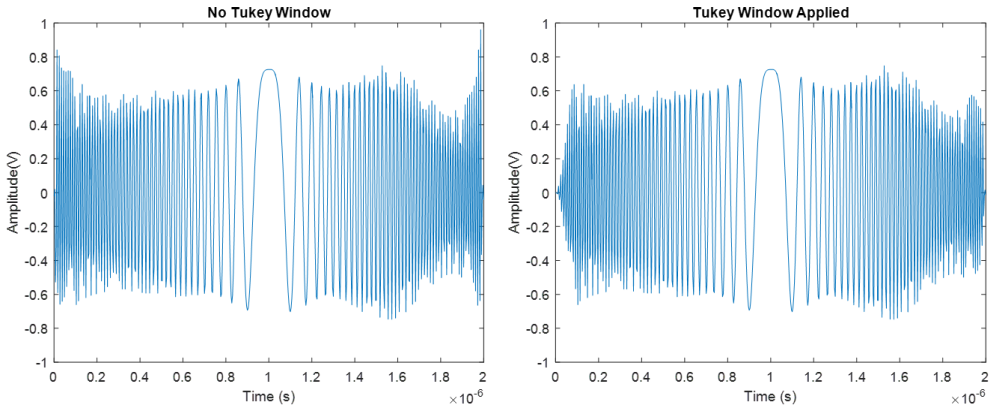

Figure 3.8: Example of Tukey Window effects

As seen in Figure 3.8, the predistorted waveform has a sharp transition on the edges that are not ideal. Additional information on the Tukey window can be found in [29].

4 Test Systems

The two test systems used to test and evaluate the predistortion technique comprised of four evaluation modules from Texas Instruments. The modules include two FPGAs, a Digital to Analog Converter (DAC), and an ADC. The waveforms designed for this system are similar to the waveforms displayed in [8]. In addition, the relationship between the FPGA and the CPU is similar to the one described in [8]. The DAC is a 16-bit, 4-channel evaluation module with an on board Numerically Controlled Oscillator (NCO). The DAC's maximum aggregate sampling frequency is 1250 MSPS. Therefore, the maximum sampling frequency for each channel is a quarter of the maximum aggregate. For instance, the maximum input sampling rate for the DAC becomes $1250/4 = 312.5$ MSPS. According to the Nyquist theorem, the max frequency that can be created by each channel of the DAC is limited to 156.25 MHz. The DAC was connected to an FPGA pattern generator that sends the waveform samples to the DAC. The waveform samples were mixed with the NCO frequency to obtain higher frequencies. The NCO worked similarly to a normal analog frequency mixer where the signal produced was the sum and the difference of the NCO frequency and the input signal. For instance, if a 10 MHz signal is mixed with a 100 MHz signal the output signals appear at 90 MHz and 110 MHz. Furthermore, signals mixed with a mixer produce harmonics at multiples of the local oscillators. For instance, the 10 MHz signal in the previous example also produces signals at the multiples of the 100 MHz mixing signals. An example of a baseband signal mixed with the desired carrier frequency of 435 MHz is shown in Figure 4.1. The signal shown in Figure 4.1 depicts the harmonics are at multiples of 870 MHz which is the clock signal fed into the DAC during this test. For the systems tested the harmonics were filtered out using low pass filters.

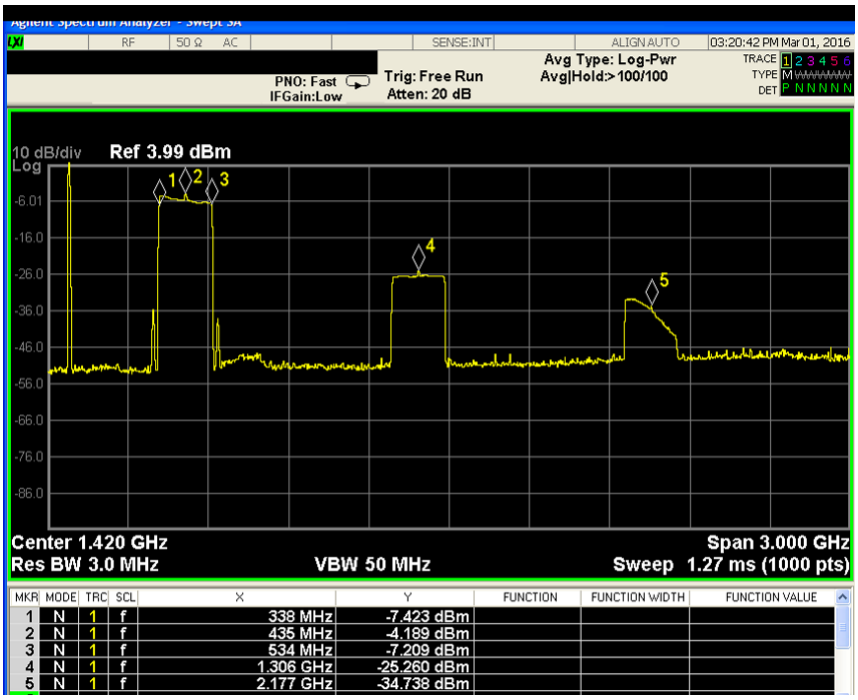

Figure 4.1: Signal Mixing Example

The filters chosen did not have a sharp enough frequency response to filter out the closest harmonic. The solution to the filter issue was to cascade two of the filters in order to achieve a sharper frequency response.

The difference between the two systems were the ADC cards used to acquire the signal. The waveforms were generated in MATLAB® and quantized to signed 16-bit words for transmission. In addition, the waveform generated was a single pulse where the designed waveform and the receive time was uploaded to the DAC. The waveform generated contained the chirp used for the radar system and receive time was represented filled with zeros. The waveform sent to the DAC is shown in Figure 4.2. In addition, the DAC subsystem functions by continuously transmitting the waveform for as long as the system is running. In other words, the DAC transmits the uploaded samples and when the last sample is uploaded the system repeats the waveform at the first sample.

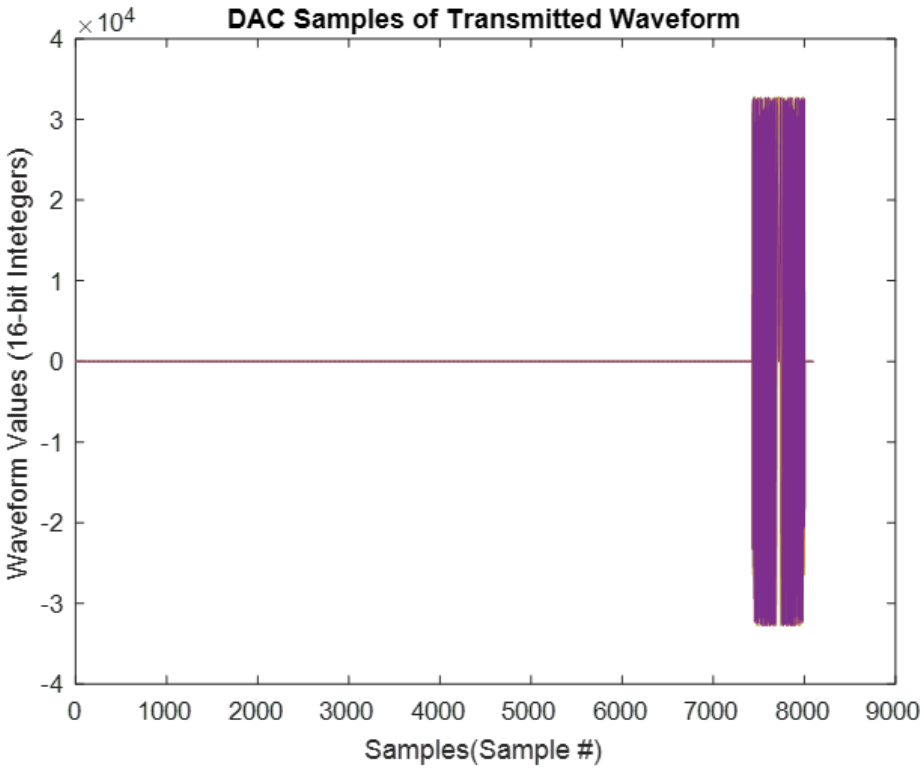

Figure 4.2: The DAC Samples of the Uploaded Waveform

The FPGA driving the DAC produced a square pulse every time the end of the pattern in transmitted. In the designed system, the square pulse was used to trigger the ADC to begin sampling. The ADC was then configured to capture a set amount of samples that would be enough to capture the reflected waveform from the desired target. In order for the ADC to begin capturing the reflected data, the trigger signal had to occur at the end of the designed chirp waveform. The desired chirp waveform was purposely placed at the end of the transmitted samples to guarantee the trigger signal was produced at the end of the chirp. The amount of zeros that were transmitted in the pattern can be varied to adjust the effective pulse repetition frequency (PRF) of the radar waveform. The maximum number of 16-bit samples that can be uploaded to the subsystem is 2097152. In addition, the samples

uploaded to the subsystem had to be in multiples of the powers of 2. In Figure 4.2, the number of samples uploaded was 8096. Furthermore, the DAC samples can be uploaded as four different column vectors with each representing a single channel of the DAC. In the system tested, the DAC was uploaded with the real part of the designed chirp signal on channels 1 and 3 and the imaginary part of the designed chirp signal on channels 2 and 4. The real part and imaginary parts were separated because the NCO expects the real part on channels 1 and 3 and the imaginary parts on channels 3 and 4.

4.1 User Interface

In both systems the Texas Instrument High Speed Data Converter Pro user interface was used to configure both the FPGAs controlling the DAC and ADC. The interface for both the DAC and the ADC could be used to configure the trigger settings of each board individually. For the DAC the trigger would initiate transmitting of the loaded waveform. However, it was found that the trigger would start the waveform pattern and continuously repeat the waveform until the system was powered off. For the designed system, the DAC trigger was not used. For the ADC, the trigger would cause the ADC to collect a specified number of samples. In the system designed this was utilized to collect the data. The trigger was configured to trigger at the end of the pattern and collect a set number of data points. In addition, the ADC interface allowed for the user to save the collected ADC codes as a csv or raw binary files. The system designed chose to use csv files for easy importation into MATLAB®. Both interfaces allowed the x-axis to be displayed as time or samples and the y-axis to be displayed as 16-bit code values or voltage values. In addition, both interfaces allowed for various other configuration that allowed the user to view data in different ways including a side-by-side view of two channels.

An image of the user interface for the DAC is shown in Figure 4.3.

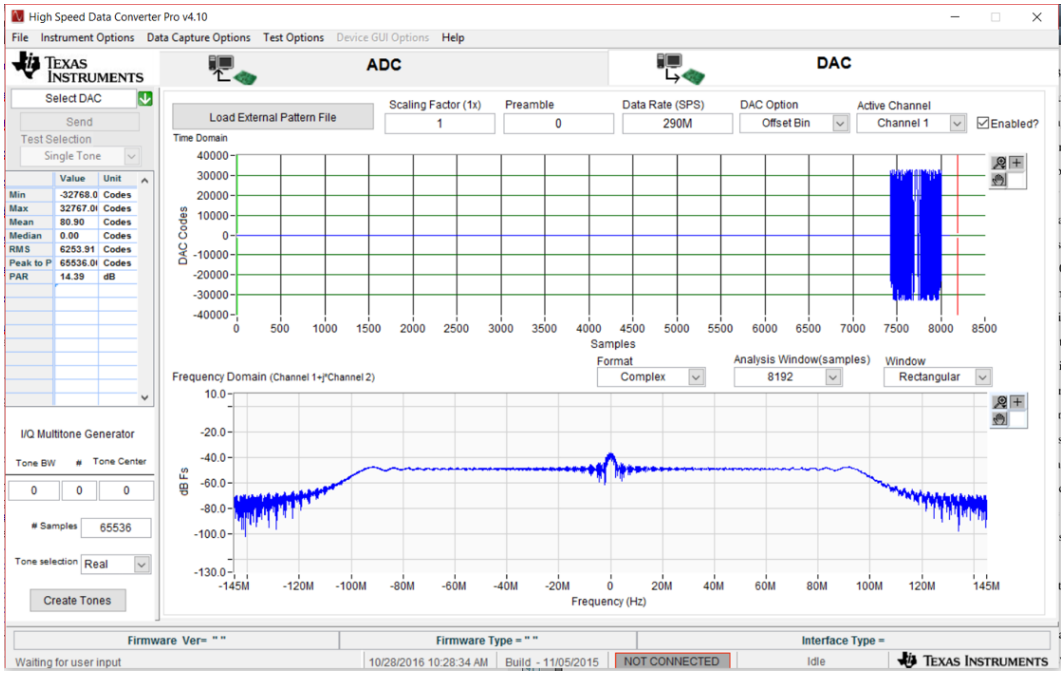

Figure 4.3: The DAC User Interface

The DAC user interface required the user to enter the DAC data rate as well as the quantization format for the waveform samples. The DAC rate was a function of the input clock as described above. The interface also allowed for a scale factor of less than or equal to one to be applied to the waveform. The scale factor could be utilized to adjust the max amplitude of the wavform. The preamble section of the user interface allowed for the user to provide a pattern to be transmitted before the waveform was transmitted. In the system designed the scale and preamble features were not used. The quantization format had two options: offset binary and 2's complement. For the system designed the waveforms were quantized in the offset binary format. The interface also allowed for certain channels of the DAC to be enabled or disabled. Furthermore, the interface allowed for users to load custom waveforms or generate basic waveforms. The system designed and tested required

the utilization of a custom waveform. The DAC interface also provided the ability to view the Fourier transform of the waveform. The analysis window allow for the view of the complex or the real Fourier transform. The complex version of the Fourier transform was calculated with the assumption that the in phase signal is on channel 1 or channel 3 and the quadrature signal to be on channel 2 or channel 4. For the real Fourier transform, the uploaded waveform on the selected channel was used in calculating the transform. The interface also allows the user to pick the number of samples to used in calculating the Fourier transform. Lastly, a window can be applied to the waveform for the calculation of the Fourier transform. The ADC interface also included an extensive amount of features for viewing the data collected from the ADC. An image of the ADC interface is shown in Figure 4.4.

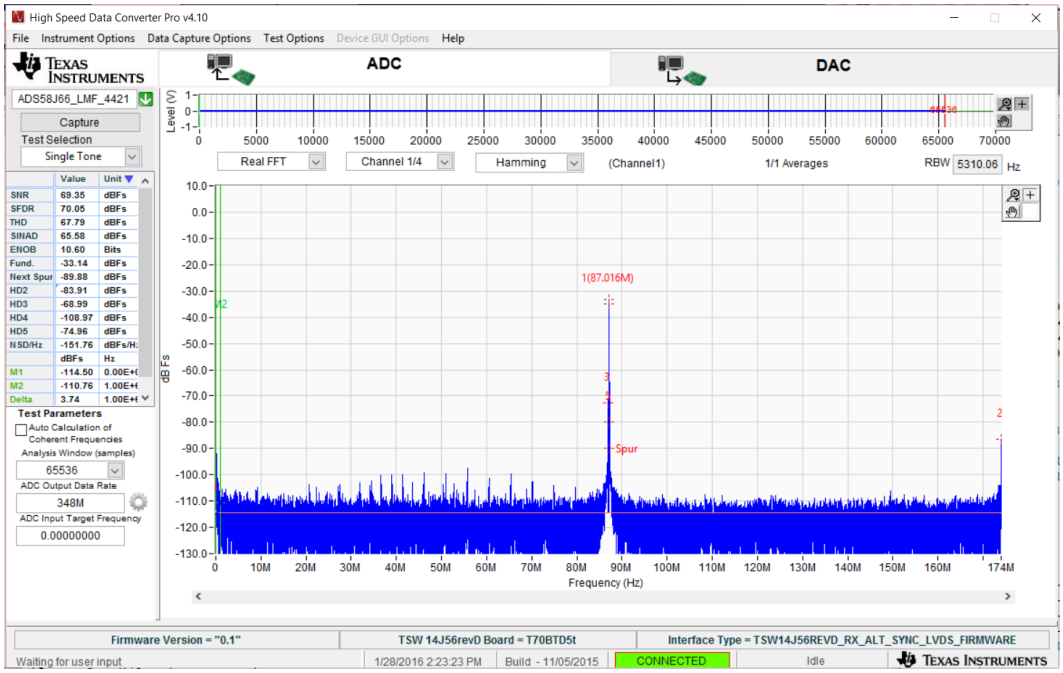

Figure 4.4: The ADC User Interface

The ADC interface allowed for the user to view the time domain signal on the top of the screen. In the bottom section of the screen, the analysis window was

similar to the DAC analysis window. The real and complex Fourier transform can be viewed in the same manor as the DAC interface. On the left, the ADC data rate was entered along with the amount of samples for the analysis window. In addition, a target frequency can be entered to center the analysis window on the desired frequency. In addition to the Fourier transform of the waveform, the interface also allowed the user to view the converted codes from the ADC as well as the actual bits converted from the ADC. The codes option allowed the user to view the time representation of the signal with more detail. Lastly, the ADC interface also allowed for the ADC to continuously capture where the graph on screen would update after a certain number of specified collections.

4.2 System A

The ADC for the first system was a 14-bit 4-channel evaluation module with an on board clock generation chip, shown in Figure 4.5. The clock generation chip created the sampling clock for the ADC. The ADC was connected to an FPGA that collected the data and displayed them to the computer screen. In the tested system the clock generation chip of the ADC was used to divide the given clock in order to achieve a synchronous clock between the DAC and the ADC to prevent phase distortions in the signal caused by an asynchronous clock. The ADC supports up to a 500 MSPS sampling rate but due to the Nyquist theorem the maximum signal that can be represented is 250 MSPS. An external clock signal was provided from a function generator and fed to both the DAC and ADC to provide a synchronous clock.

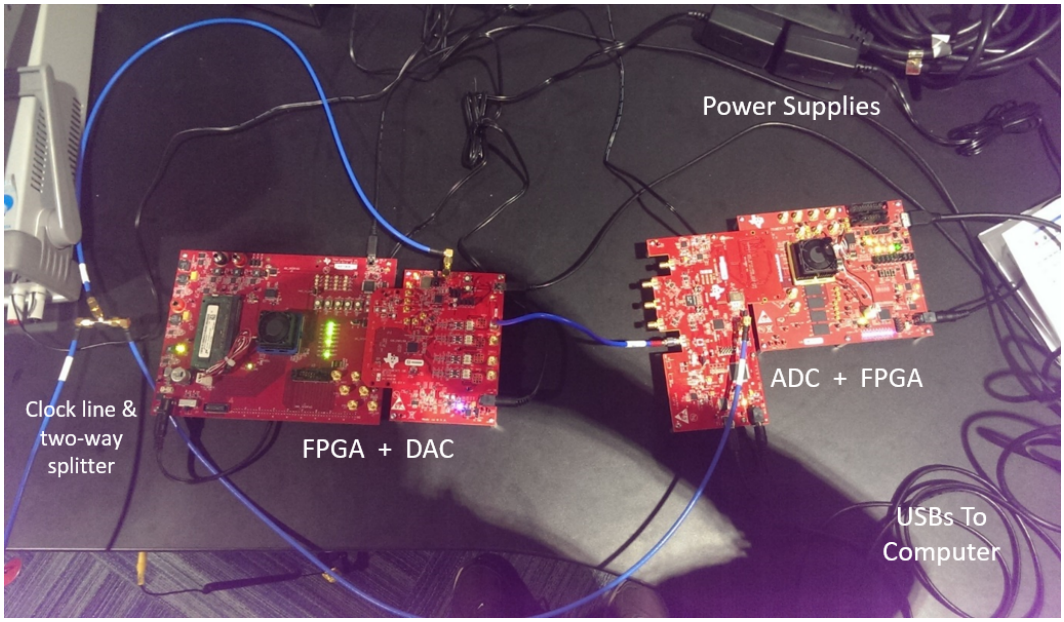

Figure 4.5: The Digital First System Used to Synthesize Radar Waveforms

The system was designed to operate at a carrier frequency of 455 MHz with a 70 MHz bandwidth LFM waveform for transmission. The pulsewidth of the system was chosen to be the popularly used 20 μs. However, due to the DAC data input rate limitation, a signal could not be created at the carrier. To create a signal in the confines of the DAC the pattern transmitted was created by at a 67 MHz intermediate frequency (IF) signal with 70 MHz Bandwidth in MATLAB® and the NCO set to a mixing frequency of 522 MHz to get a difference of $522 - 67 = 455$ MHz. The difference signal was utilized for ease of filtering and to minimize the effect of reciprocal image created by mixing signals. The frequency of the external clock was chosen based off of the ADC sampling rate. The system utilizes under sampling in order to reduce the sampling speed of the ADC and the data volume collected.

The maximum real valued bandwidth that the chosen DAC could synthesize was roughly 150 MHz due to the DAC being limited to 156.25 MSPS per channel. Three waveforms were chosen to observe the system response: 70 MHz bandwidth

centered at 455 MHz, 70 MHz bandwidth centered at 435 MHz, and 100 MHz bandwidth centered at 455 MHz. As a result, three test cases were tested on system A. Table 4.1 shows the specifications of each test case in greater detail.

Table 4.1: Specifications of Each Test Case

Test Case 1	**Test Case 2**	**Test Case 3**
70 MHz Bandwidth	70 MHz Bandwidth	100 MHz Bandwidth
67 MHz IF Mixed with 522 MHz	87 MHz IF Mixed with 522 MHz	67 MHz IF Mixed with 522MHz
455 MHz Carrier	435 MHz Carrier	455 MHz Carrier

The waveform was created in MATLAB® at a intermediate center frequency with the correct bandwidth. The waveform was then converted to 16-bit integer representations of the signal values. The waveform was then loaded to the DAC and mixed up to the desired carrier frequency using the DAC's internal NCO. The DAC's internal NCO expects a complex signal so in order to feed in a real valued waveform the NCO was set to half the external clock frequency making the complex mixer act like a real valued mixer. A Tukey window was also utilized to provide a more gradual transition for the DAC to synthesize. The DAC was then configured to have an 1044 MHz input clock with the sampling frequency set to 348 MSPS and an input data rate of 261 MSPS. The three tests explored the system's capability to create and capture higher bandwidth signals. The three test cases explored the bandwidth with the varying IF and NCO frequencies to achieve different carrier frequencies. Different carrier frequencies were chosen within P-band to prevent aliasing when under-sampled. The comparison of each test case are shown in table 4.2.

Table 4.2: Comparison of Each Test Case

Test Case 1	**Test Case 2**	**Test Case 3**
No Aliasing	Aliasing	No Aliasing
Bandwidth Achieved	Bandwidth Achieved	Bandwidth Achieved
Upper Limit Well Under Nyquist for DAC	Upper Limit Close to Nyquist for DAC	Upper Limit Well Under Nyquist for DAC
3 dB Power loss after Predistortion	3 dB Power loss after Predistortion	11 dB Power Loss after Predistortion
Small Bandwidth	Small Bandwidth	Larger Bandwidth
Small Amplitude Fluctuations	Small Amplitude Fluctuations	Large Amplitude Fluctuations

With the other two bandwidths tested it was found that artifacts in the frequency domain occur. As shown in Figure 4.6, if the IF was chosen to not allow enough guard bands of the initial waveform the DAC began to misbehave and created undesired artifacts in the received waveform. These artifacts are caused by creating waveform components that are not far enough from the Nyquist frequency. In other words, the frequencies produced began to encroach the guard bands causing the system to allow the frequency image of the waveform to begin appearing in the desired frequency band. In addition, the waveform components alias due to the under-sampling technique and the images created by the DAC. The images are under sampled as well causing artifacts like the ones shown in the right plot of Figure 4.6. In Figure 4.6, the left figure is caused by the image created by the DAC being too close to the desired waveform in the frequency spectrum. As a result, the sum and the difference results of the mixer are overlapping in the frequency domain. The overlap causes the frequency spectrum of the waveform to alias. In the right of Figure 4.6, the upper frequency limit of the waveform is close to the Nyquist limit of the under-sampling technique.

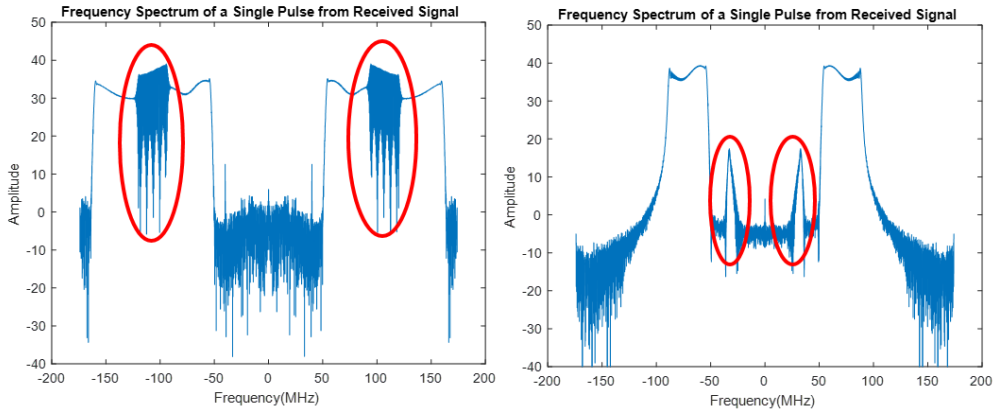

Figure 4.6: Aliasing of 70 MHz Bandwidth Signal *left* IF:67 MHz NCO:502 MHz *right* IF: 87 MHz NCO: 522 MHz

The result was some undesired spurs in the frequency domain, which were caused by the image produced by the DAC mixer, to alias into the sampled frequency spectrum. Both cases caused the predistortion technique to be unsuccessful since the phase of the waveform is distorted due to these frequency artifacts. As a result, the capabilities of system A could not support the design specifications of the desired experiment and was not chosen for the experiments conducted.

4.2.1 Received Waveforms from System A

The system response of the system was captured and shown in Figure 4.7. The 100 MHz bandwidth chirp was centered at 435 MHz and under sampled at 348 MHz with a 14-bit resolution. As seen in figure, the envelope of the waveform is not flat. The distortion to the amplitude of the waveform was caused by qualities within the DAC and ADC. For a radar system the goal is to have a flat envelope to ensure a constant power transfer across the waveform as observed by the ADC.

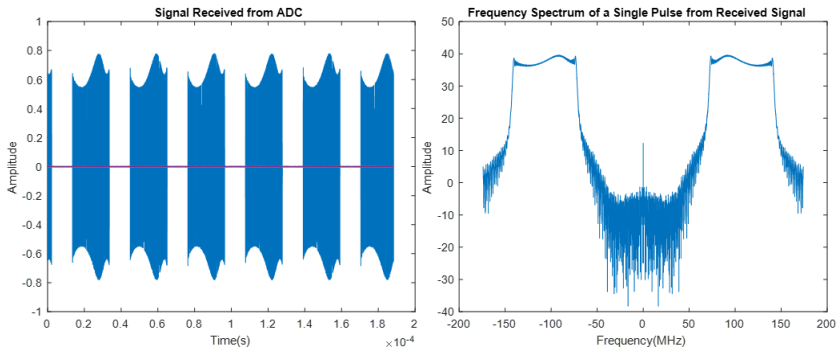

Figure 4.7: Received System Response

Irregularities in the amplitude of the waveform causes for an inconsistent output from the matched filter. For instance, the returns from the output of the matched filter are significantly less because the filter is not completely matched to the received waveform. The target could be buried in the noise floor because the matched filter is a flat envelope being correlated with the distorted waveform. This means the filter was not completely matched which decreases the amount of signal to noise gain received from pulse compression. As a result, when the radar data is coherently integrated the intensity of the target could also be buried in noise floor when the target should be prominent if the filter was matched. To ensure the maximum range of the radar, a form of predistortion can be utilized to reverse the distortion caused by the system. Since the phase of the signal is not distorted the predistortion can be the inverse of the received envelope. The envelope was calculated using MATLAB® and used as the predistortion applied to the transmitted waveform.

4.3 System B

The ADC for the second system was a 12-bit dual channel evaluation board from Texas Instruments, shown in Figure 4.8. The ADC requiree an external clock to create the sampling speed for the system. In addition, the maximum sampling speed

for the ADC was 800 MSPS per channel. Again, the ADC is limited by the Nyquist theorem making a 400 MHz signal the maximum signal that can be represented. The ADC was driven by a duplicate of the FPGA that drives the DAC. Again, an external clock signal was provided from a function generator and fed to both the DAC and ADC to provide a synchronous clock. The waveforms designed for the system were created at baseband in order to maximize the achievable bandwidth for the signal.

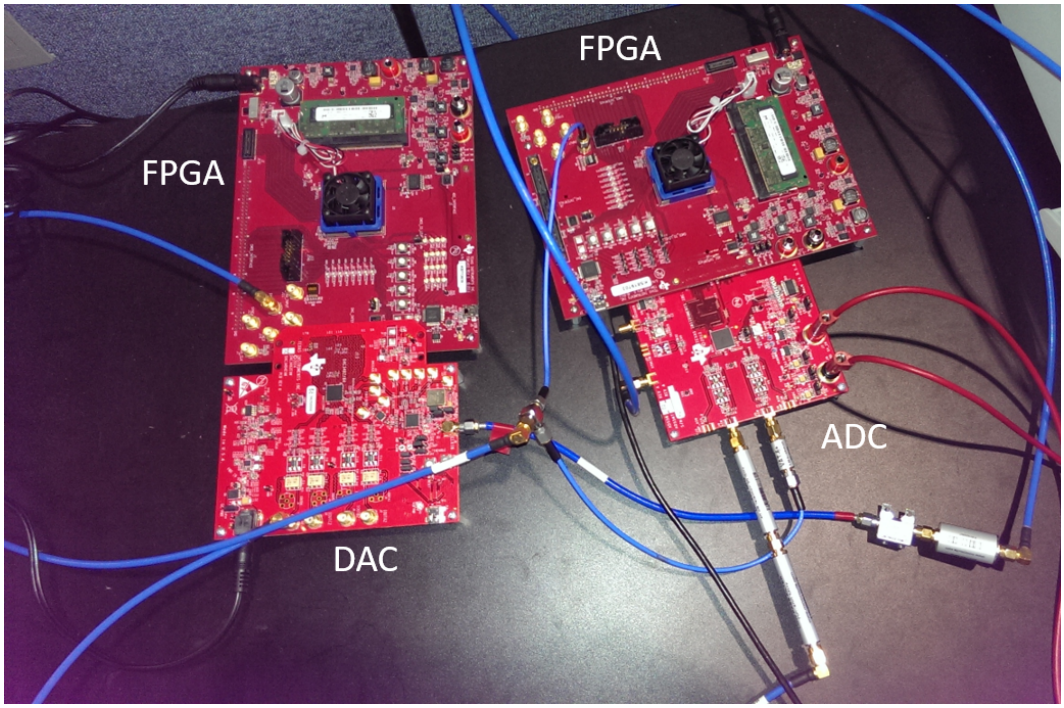

Figure 4.8: The Digital System Used to Synthesize Radar Waveforms

In addition, complex signals provide phase information for the radar. This implies that complex signals carry more information about the motion of the target (for SAR, this would be the motion of the platform). In this case, a 580 MHz clock was used to produce the sampling speed for the ADC. The system was designed to run at a carrier frequency of 435 MHz with a 200 MHz complex bandwidth LFM waveform. In addition, the application of this system needed to have a smaller blind

range since the target of interest was closer than expected. The blind range in this case was minimized by shortening the pulse length. A 2 μs pulse was used with a pulse repetition frequency of 1 kHz. The signal was created at baseband with 200 MHz complex Bandwidth in MATLAB® and the NCO set to a mixing frequency of 435 MHz to mix the signal to the desired center frequency. The difference signal was utilized to minimize the effect of reciprocal image created by mixing signals. The system utilized under sampling in order to reduce the sampling speed of the ADC and the data volume collected. As a result of undersampling the 435 MHz signal at 580 MHz, the signal is reflected across 290 MHz and is represented at 145 MHz by the ADC. The bandwidth of the signal then spans from 45 MHz to 245 MHz which falls beneath the 290 MHz Nyquist limit and the signal data is preserved.

4.3.1 Received Waveforms from System B

The received waveforms captured by system B are shown in Figure 4.9. The waveforms show the full 200 MHz bandwidth centered at the expected center frequency of 145 MHz. However, the problem still exists where the envelope is not constant. Although the system response was different the process to correct the envelope is still the same. The center frequency of the received waveform and the effects of undersampling did not contribute to the effects of the system response. The advantage of system B over system A is the abilities to capture more bandwidth and waveforms with complex components.

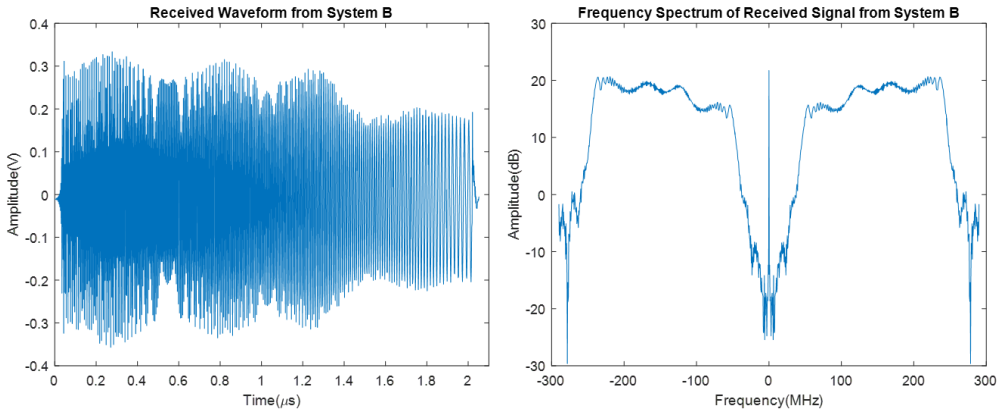

Figure 4.9: Received System Response from System B

With system B's ADC and DAC configuration the radar could determine the range of the target as well as differentiate whether the target was approaching or departing relative to the radar. In addition, with more bandwidth the radar's range resolution greatly increases and the radar can differentiate between targets that are closer together.

5 Predistortion Result

In order to test the technique, a signal was first propagated through the desired test system. The output of the DAC was fed directly into a channel of the ADC, and the signal acquired. After the signal was acquired, the predistortion technique was applied via MATLAB®. During the application of the technique, a single pulse of the received data was acquired and the envelope estimation algorithm was applied. The envelope was then inverted and applied to the original waveform sent through the system. The result of the predistortion algorithm was then sent into the system once more, and the results observed to confirm the removal of the system response. If the predistorted signal continued to produce an undesired amplitude distortion, the signal must be reconditioned with slight adjustments to the envelope estimation. These slight adjustments to the envelope estimation technique produce either a tighter or smoother estimated envelope. For this application, since MATLAB®'s envelope estimation technique uses a smoothing filter to create the envelope, the number of taps in the smoothing filter would be adjusted to produce the desired results. For instance, if the predistorted signal contained a large increase in modulus at the end of the pulse, it would likely be caused by the estimated envelope containing a near zero value at either the beginning or the end of the pulse used to calculate the system response that could not be removed by the Tukey window. When the envelope gets inverted, the near zero values would become quite large and cause an overshoot in the predistortion applied to the waveform. As a result, the waveform would become over distorted and the system response would not contain enough distortion to produce a constant modulus. More taps in the envelope estimation technique allow for the envelope to be more lenient to the sharp fluctuations on the ends of the pulse. The smoothing filter effectively causes the estimated envelope to produce more of a gradual transition along the peaks of the pulse, which in turn

could cause the ends of the envelope to increase. When the envelope gets inverted with larger end values in the envelope, the resulting predistortion contains more defined end points that lower the amount of distortion applied. This minimizes the undesired increases at the edges of the system response pulse. Variations in the modulus could also be caused by misalignment in the pulse captured. For instance, if the pulse captured for the envelope estimation were cut off or contained too many points, the envelope estimated would contain either an incomplete version of the system response or distortions not caused by the system. If the pulse was cut off the system response is not completely represented and thus the predistortion calculated does not compensate for all of the system response. Conversely, if the pulse contains too many points it will capture portions of the signal where the system was not transmitting a pulse which causes the estimated envelope to include noise as part of the system response. Both issues can be mitigated by correctly capturing the pulse needed for the envelope estimation technique. The results of the predistortion for system A are shown in Figure 5.1.

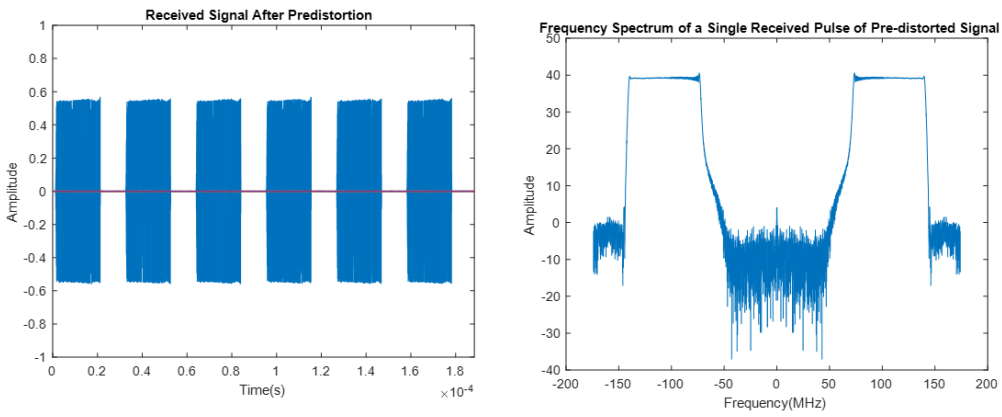

Figure 5.1: Result of Predistortion from System A

As demonstrated in Figure 5.1, the signal envelope was flat and constant, proving the amplitude predistortion technique works and was effective for this applica-

tion. While the predistortion technique worked for system A, system B operated with a different ADC and under sampling scheme which induces different distortion characteristics. The predistortion technique was also conducted for system B to confirm the change in undersampling and ADC does not introduce distortions that cannot be reversed via amplitude predistortion. In addition, the predistortion technique was used to confirm that the ADC does not produce any phase distortions. The results of the predistortion technique on system B are shown in Figure 5.2.

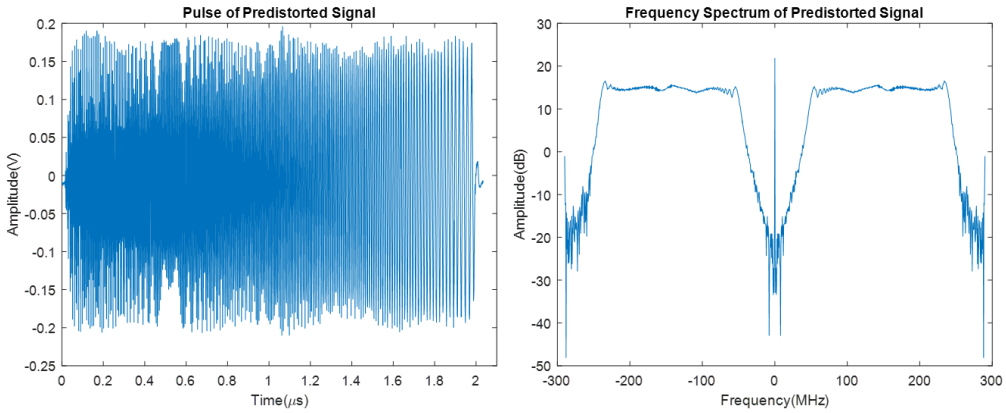

Figure 5.2: Result of Predistortion from System B

Again the resulting envelope was significantly flatter and the distortions shown previously were significantly reduced. These results show that the technique works for multiple systems with different system responses, meaning that it can be utilized in MIMO systems. For the instance depicted in Figure 5.2, the distortions caused by system B and the predistortion technique applied caused a 3 dB decrease in the power transmitted. The distortions can vary based on environmental factors causing different degrees of power loss. Although the predistortion method yields a lower power level, the predistortion technique still provided an improvement in the matched filter response. Figure 5.3 shows the matched filter response for a non-predistorted signal compared to the predistorted signal. The matched filter used to

compress the signals in Figure 5.3 was a ideal baseband chirp.

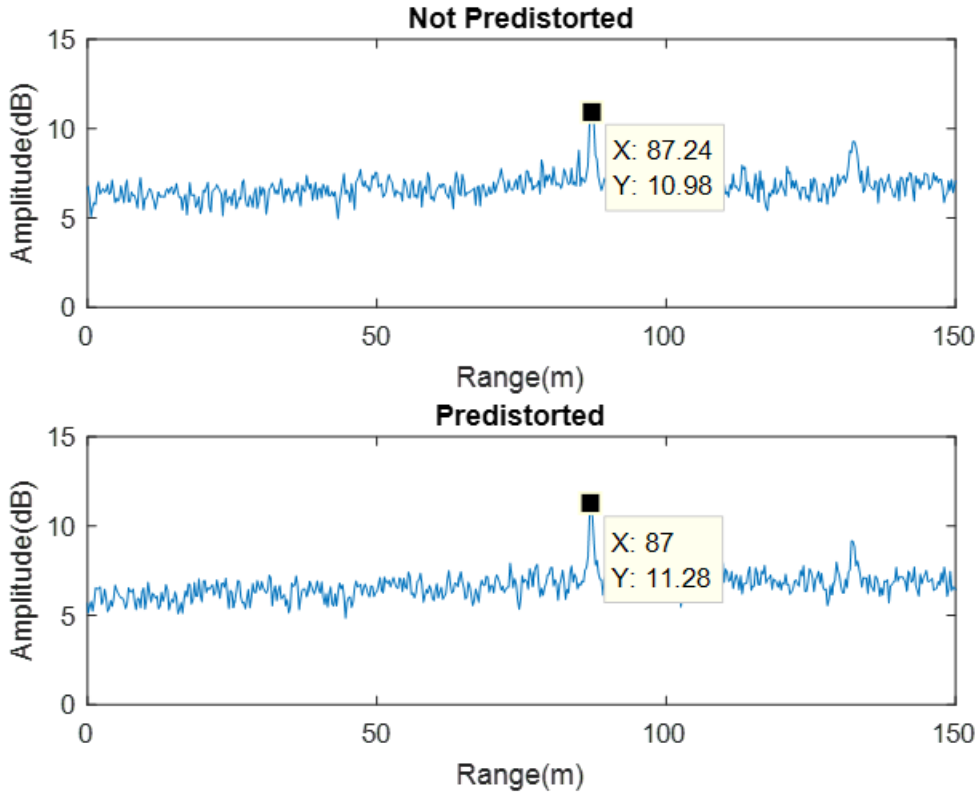

Figure 5.3: Matched Filter Response of Non-Predistorted vs Predistorted Signals

As seen in Figure 5.3, the improvement to the predistorted signal compared with the non-predistorted signal is 0.3 dB. Even with the 3 dB loss in amplitude, the predistorted signal still provided a slight improvement in the matched filter response. With a full strength signal the improvement from the matched filter response would theoretically increase proportionally.

6 High Bandwidth

The application tested required determining the range of an object 363 meters from the radar. The target was a 6 meter by 3 meter rectangular trailer placed in an open field with minimal reflections. With system A, using a 20 μs pulse and a 100 MHz bandwidth produced a blind range of 3000 meters and a range resolution of 1.5 meters. Therefore, the data collected from system A would contain unusable data even if it contained artifacts other than noise. Conversely, system B could capture 200 MHz bandwidth with 2 μs pulses, which yielded a blind range of 300 meters. The range resolution of system B allowed for the radar to detect anything placed more than 0.75 meters away from the target, as well as resolve the target into 4 range bins. As a result, more bandwidth with a shorter pulse length is desired. However, with the DAC being able to only produce complex waveforms from negative 156.25 MHz to positive 156.25 MHz, the maximum achievable bandwidth theoretically is 312.5 MHz. In hardware, aliasing begins to occur if the bandwidth limits get close to the Nyquist limit. Therefore, the theoretical bandwidth achievable in hardware has to be reduced. The gaps between the bandwidth limits and the Nyquist limit are known as guard bands. For instance, with 10 MHz guard bands the DAC can only synthesize a 292.25 MHz bandwidth signal. Although the DAC can synthesize roughly 300 MHz of bandwidth, the system bandwidth is limited to 200 MHz by the ADC acquiring the signal. With the under sampling scheme utilized in system B, the theoretical maximum bandwidth that can be acquired is 290 MHz centered around 145 MHz. However, guard bands, shown in Figure 6.1, need to be in place so that aliasing does not occur on the receive end also.

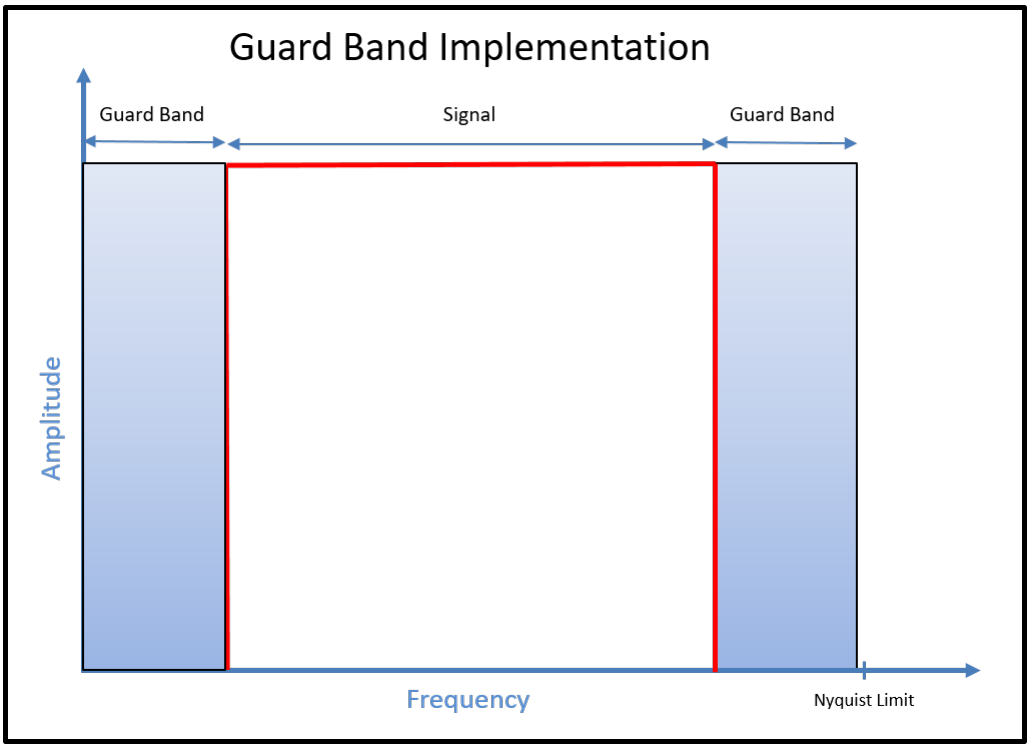

Figure 6.1: Visual Representation of Guard Bands

Due to the necessity of guard bands, the maximum bandwidth that can be acquired decreases. Through experimentation, the optimal guard bands for system B were determined to be 45 MHz meaning the maximum frequency could be 245 MHz and the corresponding minimum occurred at 45 MHz. As a result, a 200 MHz bandwidth signal was created and centered at 435 MHz so that when down sampled by system B, it would be centered at 145 MHz. The initial tests of the application inspired the experimentation with transforming the system into a synthetic aperture radar (SAR). For SAR imaging, maximizing bandwidth is key to resolving a detailed picture. SAR imaging takes the data collected from each pulse and combines them to create an image. The resolution of the image is dependent on the range resolution and the number of pulses taken in a period of time. For SAR, having a high bandwidth signal over a small pulse width allows for greater range resolution,

while also reducing the system's blind range.

6.1 Radar Equipment

The components of system B alone can not be used as a radar since the signal produced by the DAC does not have the strength to reach the target. In order to complete the radar chain, a high power amplifier, circulator, and antenna must be added, at the very least. However, since the electronics are designed to handle signals up to a power level of 1 decibel-milliwatt (dBm), protection circuitry has to be incorporated. The power level needed to reach 363 meters can be calculated using the radar range equation (6.1).

$$P_r = \frac{P_t G^2 \lambda^2 \sigma}{(4\pi)^3 R^4} \tag{6.1}$$

Where:

P_r = Power Received

G = Gain of Antenna

λ = Wavelength of the Waveform

σ = Radar Cross Section of Target

R = Range to the Target

A P-band antenna was chosen due to the frequencies created with system B. The antenna chosen was a dual ridge horn typically used for chamber measurements. Only one antenna was available, meaning that a circulator was needed in order to allow for the single antenna to be used for both transmit and receive. Furthermore, a high power amplifier was used prior to the circulator to ensure the transmit signal reached the power necessary to reach the desired target. Since the power received by the receiver was inversely proportional to range, the closer the reflector was,

the stronger the power received. On the receive side, the radar had a possibility of getting a strong reflection from a reflector that was very close to the radar. The strong reflection could have been larger than 1 dBm, depending on the reflector. In order to prevent damage from these large reflections, a limiter was used to make sure the power does not exceed the 1 dBm limit of the ADC. Conversely, since power reflected from the target at the given range is calculated by ignoring losses in propagation, the power received at the maximum range was actually quite low and in order to produce a higher signal to noise ratio, a low noise amplifier was used to boost the signal a small amount before being acquired by the ADC. The high power amplifier chosen was manufactured specifically for P-band implementation and is rated to produce 33 dB of gain. In addition, the antenna chosen was specified to produce roughly 9 dB of gain at the given frequency band used. Estimating that the target trailer had a radar cross section (RCS) of 0 dB and using the center frequency of system B for the wavelength, the power reflected was calculated (using equation (6.1)) to be -84 dBm. The LNA chosen produced 32 dB of gain, making the total power received by the ADC about -53 dBm. The system designed is shown in Figure 6.2.

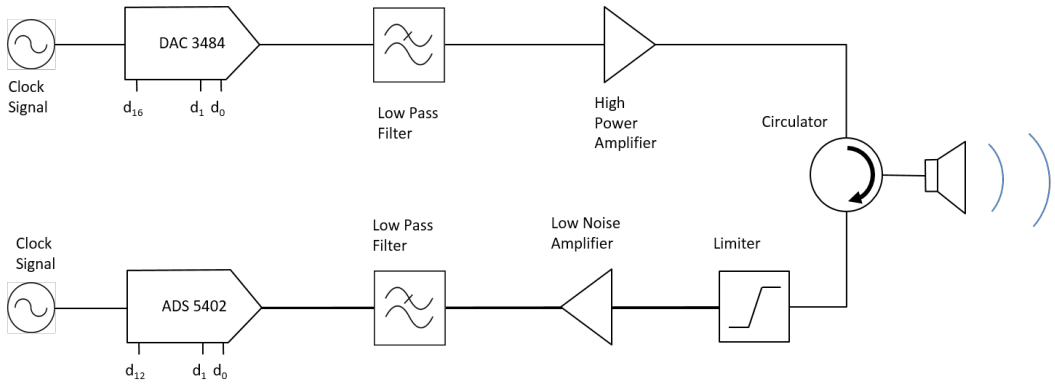

Figure 6.2: P-band Radar Design Photo Courtesy of Dr. Uysal

6.2 Amplifier Distortions

As a result of adding additional components to the system, the pre-distortion results used previously were no longer valid. Since the predistortion to remove a system response is dependent on the system, the process must be repeated if any changes are made to the system. In the P-band design, an antenna, limiter, circulator, low pass filters, and two additional amplifiers were added to the system. The high power amplifier added in the P-band design is shown in Figure 6.3.

Figure 6.3: High Power Amplifier

For the most part, the components added all introduced additional amplitude distortions into the system response that needed to be removed. However, amplifiers can introduce phase distortions if not carefully used. Amplifiers have a non linear relationship between the power fed into the amplifier and the power outputted by the amplifier. The relationship can be graphed into two sections, the linear re-

gion and the compression region. The linear region is where the amplifier outputs the expected power amplification of the power in. In the linear region, the amplifier generally behaves very close to how an "ideal" amplifier will behave. The linear region typically produces only an amplitude distortion in the system response. As a trade off of operating in the linear region, the amplifier does not operate at maximum efficiency. The efficiency of the amplifier can be determined by comparing the energy used to power the amplifier versus the amount of power gain achieved by the amplifier. When the amplifier operates in the compression region, the expected gain produces the most efficient application of the amplifier. However, in the compression region the amplifier begins to misbehave as the internal hardware of the amplifier cannot produce the specified gain for the input power given. As the input power to the amplifier begins to approach the compression region, the amplifier struggles to apply the specified gain to the signal and the output begins to drop below what is expected. Amplifiers often have a specification that designates when the compression produces a 1 dB deviation from the expected output called the 1 dB compression point. For instance, if an amplifier with a gain of 30 dB is fed with a 10 dBm signal, the amplifier will produce close to a 40 dBm output in the linear region. Conversely, in the compression region, the output power can begin to taper. This means that if the same amplifier were fed with a 20 dBm input, the output would become something on the line of 49 dBm at the 1dB compression point. A visual representation of a power amplifier curve is shown in Figure 6.4, where the expected or "ideal"output was plotted against the measured result of a high powered amplifier.

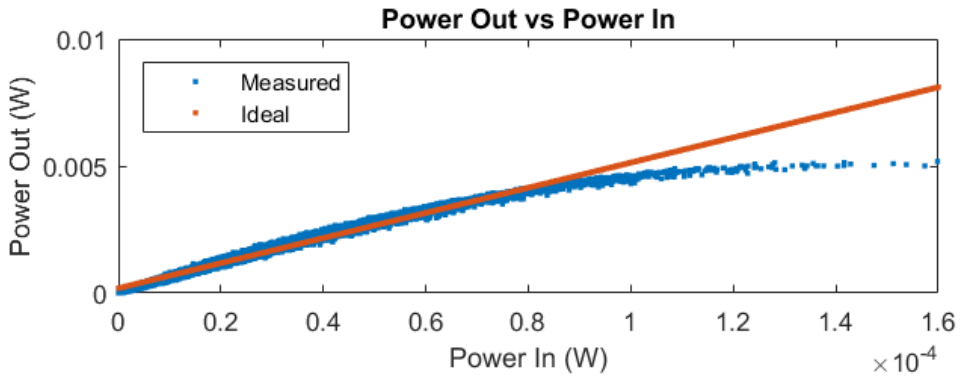

Figure 6.4: Power Out vs. Power In Curve for Amplifier

As shown in Figure 6.4, the actual power output begins to deviate from the "ideal"or expected output of the amplifier. In the compression region, the system distortion introduced begins to contain phase components, meaning the proposed method of amplitude predistortion becomes invalid. The idea of predistortion can still be applied,but using the inverse of the signal modulus would not completely remove the effects caused by the system should those effects include phase distortions.

7 High Power Amplifier System Response

For the P-band implementation, the high power amplifier utilized was kept in the linear region to lower the chances of phase distortion caused by the compression characteristics of the amplifier. In order to operate the high power amplifier in the linear region, the signal being fed into the amplifier had to be the kept at a power level low enough to keep the amplifier in the linear region. For the designed system, the the maximum output of the DAC was well within the power levels for the amplifier to be operating in the linear region. The system response removal technique was applied by creating a "loop back" scenario to acquire the signal for envelope estimation and predistortion. The loop back scenario required feeding the transmit signal after the amplifier directly into the receive chain of the radar. For a complete loop back test, the signal should theoretically pass through every component used in the system to get a complete system response. However, not all components in the system can be included in the loop back test. For instance, the antenna can not be used in the loop back test since there is no way to ensure all of the energy sent out of the antenna is fed back into the antenna without damaging the ADC. In addition, the circulator's sole application is to prevent power from leaking into the receive chain during transmit, and thus it cannot be included in the loop back test. While they could not be included in the test, both of these components produced negligible changes to the system response. The test system used to test the predistortion technique with a high power amplifier is shown in Figure 7.1.

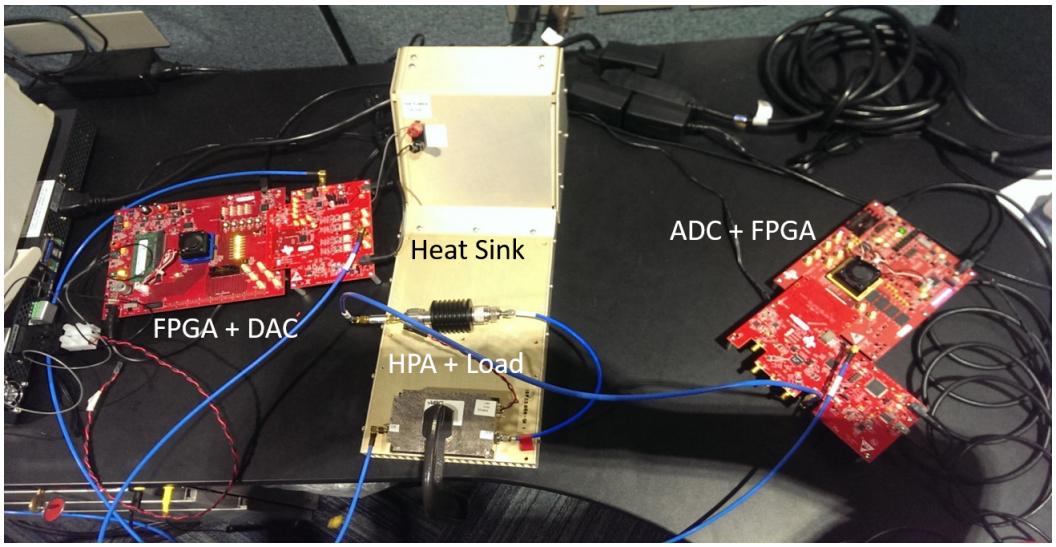

Figure 7.1: System a with Amplifier and Load

Due to the amount of heat the high power amplifier produces, the amplifier had to be placed on a heat sink to dissipate the heat. With the circulator and the antenna removed from the system, there was no component to absorb the power from the high power amplifier. In practice, the energy from the amplifier would be attenuated as it propagates through the air and was reflected back from the target. During the loop back scenario, the target and air propagation is removed from the system, and thus the signal was not attenuated and could not be safely fed into the ADC. In order to simulate the loss that occurs during propagation, a high power attenuator was connected in place of the circulator and antenna. The signal was then propagated through the system and captured using the ADC. The predistortion technique was applied using MATLAB®. The predistorted signal was then sent through the system and observed to confirm the removal of the system response. The results are shown in Figure 7.2.

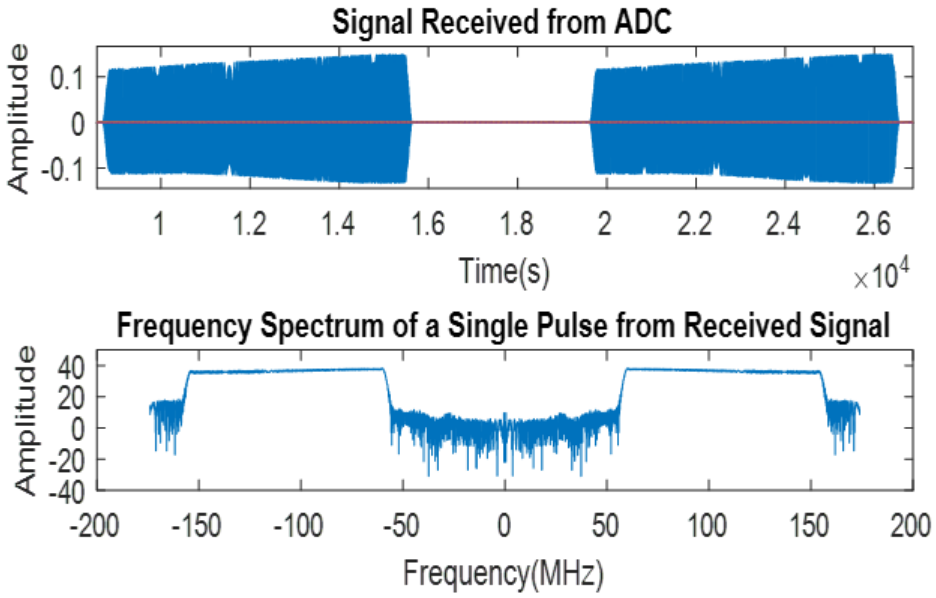

Figure 7.2: System Response with High Power Amplifier

Once the system response was determined to be sufficiently removed, the pre-distorted signal was sent through the system once again. The acquired results with the antenna and circulator were then saved off to be used for the matched filter in the radar application. The high power amplifier test was repeated for system B and the results are shown in Figure 7.3. The results in 7.3 further confirm that the high power amplifier used in the test system introduced distortions that can be removed via the technique proposed.

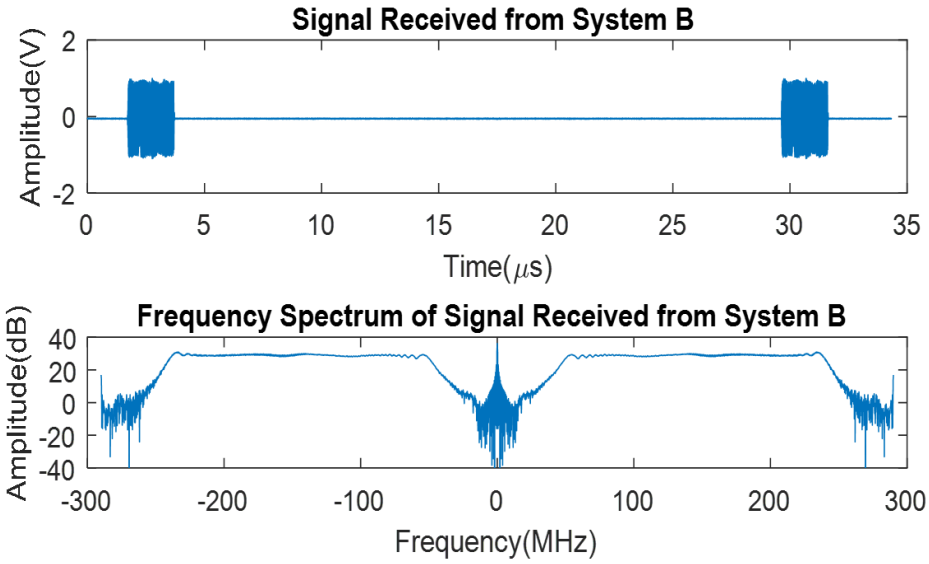

Figure 7.3: System B Response with High Power Amplifier

8 Ku-band

The radar system designed had complications in testing. The antenna originally chosen for the P-band design quickly became impractical for the desired application. The P-band antenna on hand was designed for taking measurements in an anechoic chamber and not for outdoor measurements where the ground and multipath reflections issues become apparent. The chamber accessible at the University of Oklahoma was not large enough to simulate the range to the desired target. In addition, the P-band antenna was quite large, with dimensions of 1068x585x870 mm, and became very cumbersome to transport to the desired transmit platform. While the radar system originally designed operated in the P-band, locating a set of antennas to test the efficiency of the system was not feasible. The solution was to modify the system to include two standard gain horn antennas and a UHF to Ku-band up/down converter. The inclusion of the on hand up/down converter was used to up convert the waveform in order to reduce the antenna size. Two Ku-band standard gain horn antennas were easily acquired, and the P-band radar design was converted and modified to utilize the up/down converter, as well as the two standard gain antennas. A picture of the up/down converter and the horns are shown in Figure 8.1.

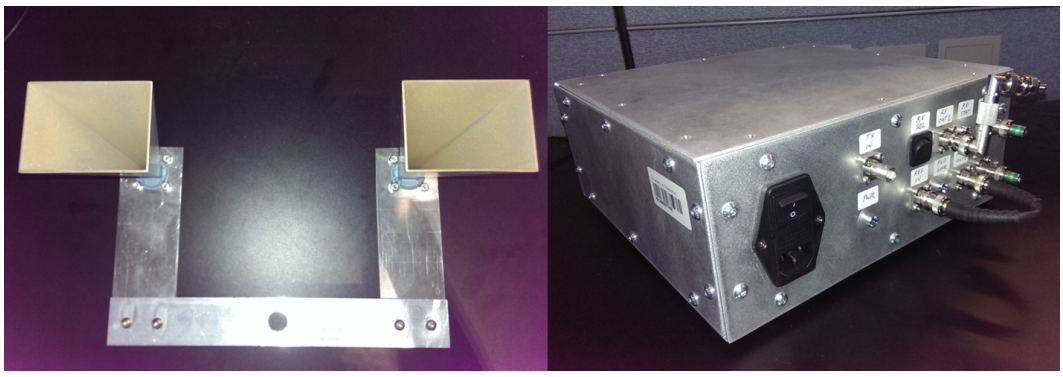

Figure 8.1: *left:*Standard Gain Horns *right:*Ku Up/down Converter

The up/down converter contained an amplifier capable of producing the 30 dBm signal required to reach the desired target, meaning the amp chosen for the P-band design could be removed. In addition, the up/down converter allowed for two antennas to be connected, one for transmitting and one for receiving. The two standard gain horns were utilized together to eliminate the need for the circulator. On the receive chain, the up/down converter contained a limiter and a low noise amplifier. This produced the power needed to safely feed the signal into the ADC, which allowed for the removal of both the limiter and low noise amplifier used in the P-band design. The modified Ku-band system is shown in Figure 8.2.

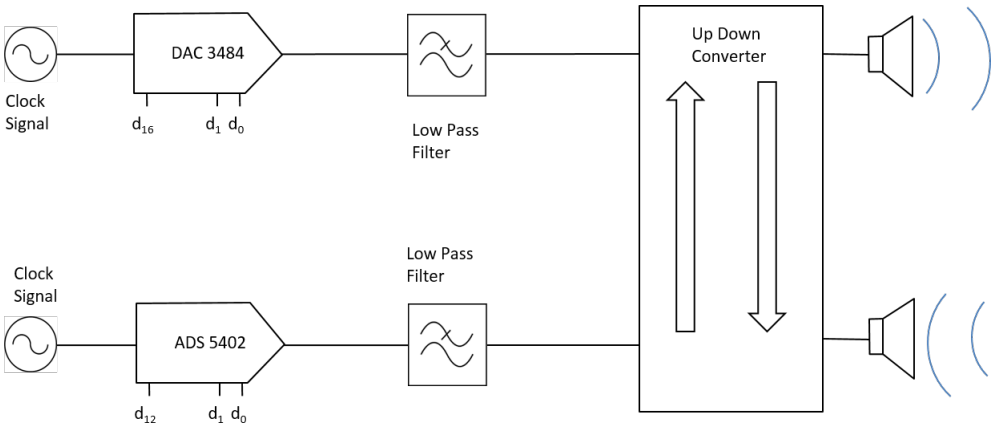

Figure 8.2: Modified P-Band Design to Incorporate Up/down Converter

The inclusion of the up/down converter effectively shifted the carrier frequency up to 13 GHz. However, since the converter reverses the conversion on the receive chain, the technique for predistortion still applied as long as the up/down converter was included during the predistortion calculation. In fact, with the converter, the antennas became the only component that was removed from the system during the loop back scenario. In place of the removed antennas, the high power attenuator was used once again to simulate the loss accrued when the waveform propagates through the air.

8.1 Radar Implementation

The Ku-band implementation was initially used as a range radar to prove the functionality of the designed system. The desired target to detect was still the trailer placed at 363 meters away from the transmit platform. The radar was placed on the balcony of the Radar Innovations Lab at the University of Oklahoma, and the target was placed on the other end of a field at the specified distance. The radar antennas were mounted on a tripod that allowed for adjustments in elevation angle, height, and azimuth. The radar antennas were pointed at the target using levels and laser range finders to ensure the target was well within the radar's line of sight. The initial test showed the desired target produced a weak reflection to the radar and it was not immediately clear the target was detected. In order to ensure the radar system was not the issue, corner reflectors were placed at various distances much closer to the radar to ensure the radar was detecting targets as expected. The scene for the radar field taken from Google Maps® is shown in Figure 8.3.

Figure 8.3: Radar Testing Enviroment

The initial results from the corner reflector targets were positive, and the data

collected clearly showed two targets at the correct distances. In addition, the field contained a number of other scatterers, including a couple of goal posts and a fire hydrant. All of the scatterers were believed to be detected by the radar. The corner reflectors were placed in two configurations, which were compared to the radar data with no corner reflectors present. In the first configuration, the first corner was placed reflector roughly 120 meters from the radar and the second was placed about 20 meters beyond the first, or 140 meters from the radar. The second configuration was nearly identical to the first, except that the second corner reflector was placed at roughly 160 meters from the radar. Each test utilized the predistortion technique, and the range results were captured and post processed using the match filter acquired during the last step of the predistortion technique. In addition, the power level of the radar was varied using the gain of the NCO within the DAC. Measurements were taken with the gain at both max power and half power to confirm the results gathered matched expectations for the range and power level of the radar system. The result of the max power test is shown in Figure 8.4. It was found that the gain set at max produced the most prominent and consistent results with the expected output. It was later found that the radar detected these targets in the blind range. With further analysis, it is believed that the complete waveform was not reflected but instead a portion of the waveform was reflected. The frequency spectrum of the received waveform showed that the radar received enough of a partial bandwidth to resolve the corner reflectors at the specified distances.

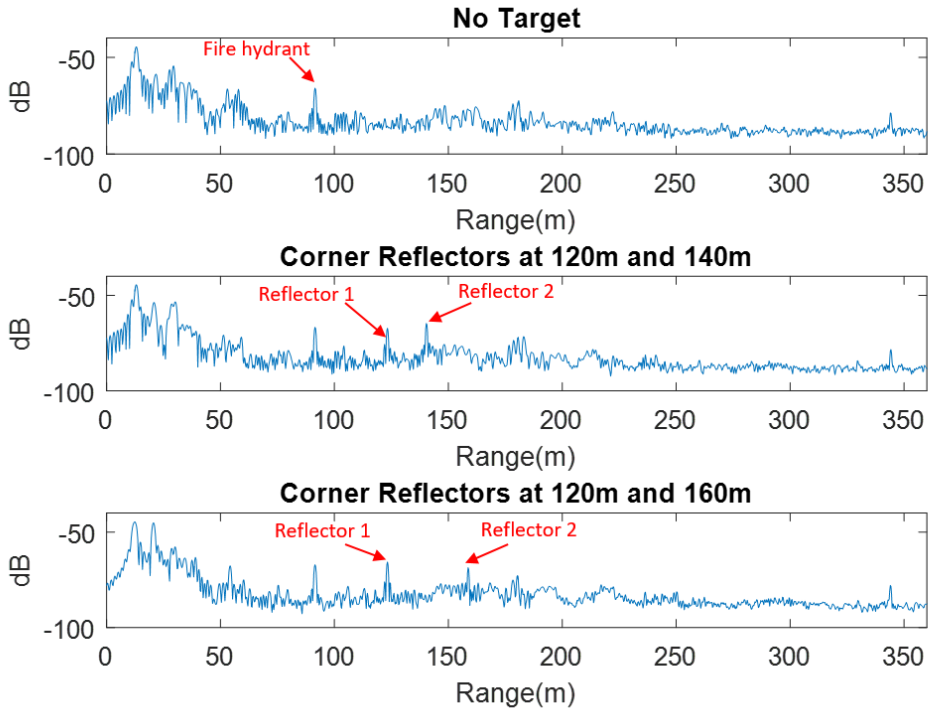

Figure 8.4: Range Result at Max Power

After verifying that the radar was functioning as expected the data was recaptured a number of times using the maximum gain with no corner reflectors present. Post processing consistently showed what was believed to be targets in the same location. In order to confirm the observed targets, the concept of coherent integration was utilized to prominently distinguish the targets from the noise floor. The concept of coherent integration is a post processing technique used to improve signal to noise ratio. The concept improves the signal to noise ratio by summing multiple pulses captured by the radar with the assumption that noise artifacts will be reduced when summed. The underlying theory is that noise is a zero-mean random process with small values that fluctuate, and when they are averaged together the positive and negative components destructively cancel themselves respectively. In

other words, when the values of the zero-mean random process are averaged, the average converges to the mean of the random process. The reason that the reflections from the targets do not also diminish as they are averaged is because these signals are constantly returning the same value. When averaged, these signals will give the mean value of the returned strength from all the pulses. Furthermore, the application of coherent integration of multiple pulses allows for signals that may be buried by the noise floor to be extracted to a detectable level as the noise floor is decreased. After the measurements were taken, the rectangular trailer was targeted once again, and additional measurements were taken and post processed. As the processed data was observed it was found that a peak appeared around the range of the target which had a weak reflection. In order to confirm the signal was indeed the desired target, coherent integration of multiple pulses was utilized in order to prominently confirm the target was acquired as shown in Figure 8.5.

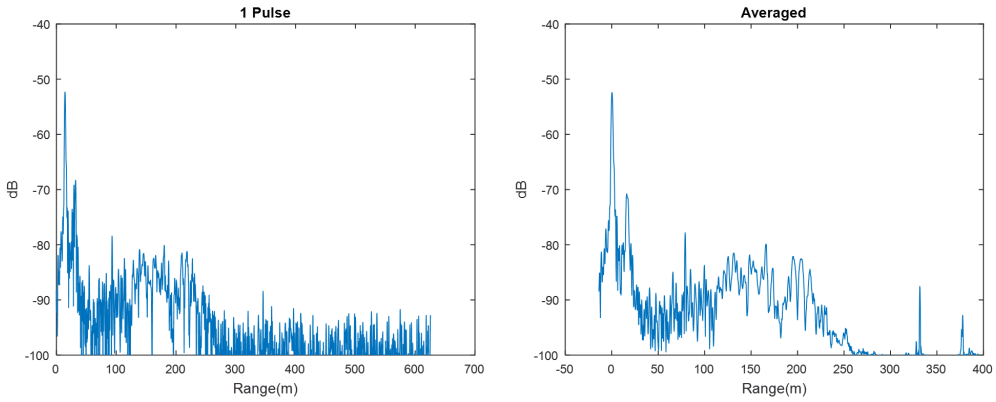

Figure 8.5: Comparison of Coherent Processing

8.2 Range-Doppler

When the target was confirmed to have been detected by the radar, the concept of producing a range-Doppler map became a realizable goal. The basic idea of a

range-Doppler map is to collect data from a radar detecting a moving target, and processing the data in such a way that shows both the range and Doppler shift of the target. Range-Doppler maps use the Doppler shift that changes from pulse to pulse and plot them against the detected range of the target. The range-Doppler map will plot all stationary targets on a single line, regardless of range. The targets used in creating a range-Doppler map have to be moving either toward or away from the radar. In order to create a range-Doppler map with the current setup, a target traveling at a constant velocity had to be detected by the radar. The data was collected from each pulse as the object moved and was observed in phase and range. The system designed with the Ku-band up/down converter and system B is shown in Figure 8.6.

Figure 8.6: System Used for Range Doppler Measurements

The system was driven by a function generator to create the clock used by both

the DAC and ADC. Data from the radar system was gathered on the laptop and processed using MATLAB®. Due to the blind range of the radar system, detecting a target traveling at a linear velocity toward the radar was unrealistic. In order to achieve a constant velocity, a trailer target was placed on a revolving turntable and revolved at a speed of 1 revolution per minute. As the target moved, the range of an arbitrary point on the target varied as the point moved toward and away from the radar. The point's radial velocity could be converted into a linear velocity that could be detected by the radar. In addition, when observed in phase the same point had a positive phase change when it was moving toward the radar and had a negative phase change as it was rotating away. This phenomenon generated two targets in the range-Doppler map, one traveling away from the radar and one traveling toward the radar. The radar was limited in the data that could be collected since the evaluation module used would not spool the data out off the on-board memory fast enough to capture one full rotation. With the system collecting data as fast as it could pipe the data to the computer, the system could only capture a fraction of a second of data. A range-Doppler map of the test is shown in Figure 8.7. The target scene included a pole placed about 30 meters in front of the target. In addition, the range-Doppler map shows that the target is rotating since the phase is not zero. The target is also slightly fluctuating in range, which is another indicator of a moving target. Range-Doppler maps take a significant amount of processing, since the range is extracted from the time it takes for a single pulse to return from the target, where as the phase is extracted from the change in phase between each pulse. Since the range and phase of the target is extracted from two parts of the same data, the data must be processed twice in order to produce the correct result. In addition, while the range can be extracted from one pulse, the phase must be extracted using two pulses.

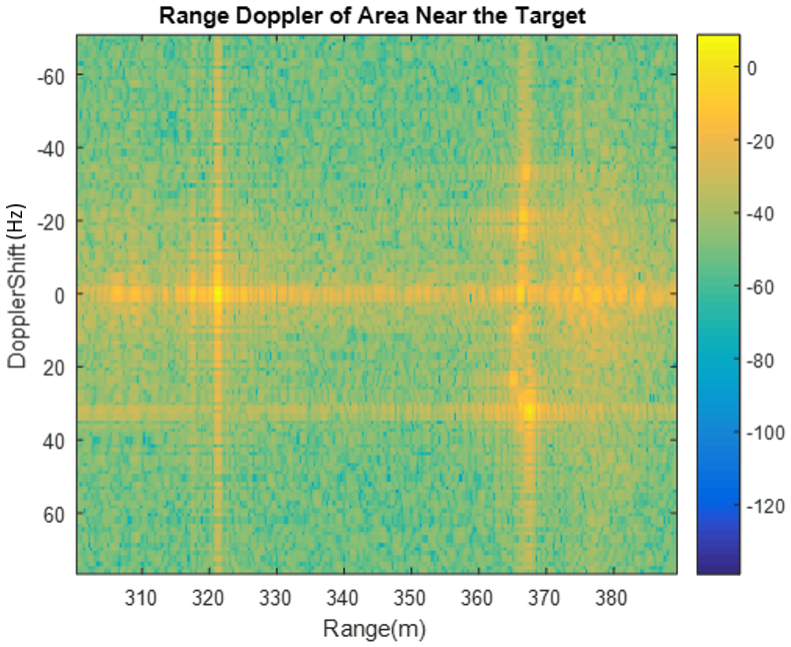

Figure 8.7: Range-Doppler Map of Area Around Target

The data can be arranged in such a way that allows for quick processing using the innate properties of the Discrete Time Fourier transform. The data must first be classified into two different time frames, fast time and slow time. Fast time is the time frame from when the transmit pulse ends to when the complete waveform is reflected back. Slow time is the time from the when the reflected pulse is received to when the next reflected pulse is received. Furthermore, the time between samples for each time frame are different. Fast time samples are spaced by the time in between samples acquired by the ADC, where as slow time is spaced by the in between transmitted pulses. The data is arranged by placing the collected fast time samples on the horizontal axis and placing the slow time components along the vertical axis. Arranging the data with slow time on the vertical axis and fast time on the horizontal axis allows for the transformation from time to frequency components by utilizing one two-dimensional Fourier transform. The two-dimensional

Fourier transform can be utilized because the fast time and slow time samples are in the time domain. In order to extract range, a matched filter must be applied to the fast time samples in order to produce a single reference point for calculating the time it took for the waveform to travel to the target and back. In addition, the slow time samples need to be transformed into the frequency domain in order to pinpoint the exact speed of the target. Furthermore, the phase can be represented as shown in equation (8.1).

$$w(t) = 2\pi f t \tag{8.1}$$

Where:

$w(t)$ = Time Varying Phase

f = Frequency

t = Time

However since the target is rotating, one side of the target will produce a negative phase change and the other side of the target will produce a positive phase change. Since there are two phase changes occurring, when the data is transformed into the frequency domain the phase offset displayed in the plot will show both negative and positive values corresponding to positive and negative speeds. When the finished result is plotted, the target will show a signature at the expected range as well as two other signatures. The two additional signatures represent the point of the target that is the closest to the radar and the point of the target that is the farthest from the radar with the respective positive and negative phases. In addition, the speed of rotation can be extracted from the phase by using equation (8.2).

$$v(t) = \frac{F_D \lambda}{2} \tag{8.2}$$

Where:

v = Velocity

λ = wavelength

F_D = Doppler Frequency

t = Time

As shown in Figure 8.7, the Doppler shift induced by the target was roughly 31 Hz. Using equation (8.2) with a center frequency of 13 GHz, the velocity from the received data becomes $0.3577\ m/s$. Furthermore, the target had a radius of 3 meters and was spinning at a rate of 1 revolution per minute. Using equation $v = \omega r$ where ω is the angular velocity and r being the radius, the linear velocity of the target becomes $0.3142\ m/s$. The velocity retrieved from the range-Doppler data corresponded to the true velocity of the trailer, showing the system correctly detected and represent the moving target.

9 Conclusion

The predistortion technique presented allows for improvement in the matched filter response. The range-Doppler map, created from the radar detecting a moving trailer target, accurately represented the target scene with the correct Doppler frequency and at the correct range. The predistortion method proposed removed distortions caused by a non-constant amplitude modulus. In addition, the system designed successfully utilized the predistortion technique. The technique also showed that as long as the distortions were constant for every pulse, the predistortion can be calculated from a single pulse and used to predistort all pulses created. The technique was also proven and implemented with low cost, off the shelf, evaluation level radar components, showing that the technique can be implemented easily on base level radar components.

The predistortion technique showed versatility in systems as the technique held true for changes in and different configurations of the system. The predistortion technique was proven with system A described earlier in the work, and was then initially tested with system B. Both systems showed a more constant modulus waveform after the application of the technique. The system independence characteristic is particularly useful in multiple element systems where the technique can be applied to the waveform generated by each element. In addition, the configurations of both systems differed in the receive chain. The system was then tested with a UHF to Ku converter containing an array of various RF components. The technique showed that adding RF components to the system, including high power amplifiers, does not introduce distortions that cannot be predistorted. The use of the converter also shows that the technique can be used for systems which utilize traditional converter chains but synthesize waveforms using digital electronics.

The system designed successfully utilized the under sampling theorem in con-

junction with the predistortion technique. In addition, the technique showed that undersampling the waveform did not affect the results obtained by predistorting. In testing the two systems described, the predistortion technique showed that changes in bandwidth do not change the effectiveness of the technique. Furthermore, the predistortion technique also showed frequency independence; as the frequency varied, the technique still produced promising results.

The system designed showed the Doppler representation of the used waveform to be consistent with the ambiguity function of the utilized waveform. The results obtained indicated that the predistortion technique could be utilized in MIMO phased array systems that utilize individual excitation circuits for each element. The technique would allow for all elements in a phased array to have a constant modulus. Furthermore, phased arrays that utilize beam steering could incorporate the predistortion technique to simplify the beam forming algorithm. For instance, a phased array system could utilize a more textbook beam forming algorithm, as the waveform modulus would be closer to an ideal waveform. In addition, the beam forming algorithm could apply a more constant amplitude change, if necessary.

The predistortion algorithm proposed in this work opens new doors to waveform generation and allows for more ideal waveforms to be easily synthesized by modern day digital electronics. In addition, the technique allows for multiple element radars to more reliably propagate the same waveform.

10 Future Work

With the promising results of the technique designed, the next step is to add some additional tests to exercise the technique proposed. An inertial measurement unit (IMU) is being obtained and the system designed will be used in a SAR application. The effects of a moving radar will be observed with the predistorted waveforms. In addition, airborne systems tend to operate for longer meaning the distortions could change gradually as the system undergoes climate and environment changes. A periodic approach would be of interest here where the predistortion technique could be applied multiple times during the observation period. The periodic approach would allow for the system to obtain the new system response, calculate a new predistortion, and apply it to the transmitted waveform. Ideally, the periodic approach would be done in real time as the system is operating to maximize the time observing.

Intuitively, the period of the periodic approach should be dependent on the application. For applications like the EcoSAR system designed by NASA, the period could be once every few seconds. This means that the predistortion technique would be applied once ever few thousand pulses. The idea is to periodically toggle a circulator to feedback an attenuated version of the transmitted waveform into the received channel so that and the predistortion technique can be applied. The new predistortion would then be applied for the next few thousand pulses and the process would repeat again on the next period. In addition, the technique would have to use an iterative approach, since the transmitted waveform is different every time the predistortion technique would be applied. For instance, an ideal waveform is transmitted for the first time the waveform is predistorted by the technique. The next time the waveform is to be predistorted, it will be using the predistored ideal waveform. The predistortion for the second iteration would no longer be applied

to the ideal waveform, but rather the predistorted ideal waveform.In order to implement the periodic approach, the technique would need to be implemented on an embedded system.

The predistortion algorithm currently predistorts the signal, and reflected data is collected for a specified time duration. The data is then post processed to obtain the range and Doppler information of the detected targets. Implementation on an embedded system would allow for the post processed portion to be removed and the data could be processed in real time. This means that the pulse compression processing utilizing the matched filter could be captured in real time. The embedded system could also be independent from MATLAB®, where instead of utilizing MATLAB®'s envelope estimation algorithm, a similar algorithm could be used to utilize the Hilbert transform and median filter to obtain similar results. Ideally, the iterative periodic adaptation to the predistortion technique utilized here would allow for an airborne radar to adapt to changing conditions, such as temperature during the plane's flight, that could change the system response.

References

[1] H. Hsiao and et. al, "A 77-GHz 2T6R Transceiver With Injection-Lock Frequency Sextupler Using 65-nm CMOS for Automotive Radar System Application," *IEEE Transactions on Microwave Theory and Techniques*, vol. 64-10, pp. 3031–3048, Oct. 2016.

[2] M. I. Skolnik, *Introduction to Radar System, 3rd Edition*. McGraw-Hill Education, 2001.

[3] C. Fulton, M. Yeary, D. Thompson, J. Lake, and A. Mitchell, "Digital phased arrays: Challenges and opportunities," *Proceedings of the IEEE, invited paper*, vol. 104, pp. 487–503, Mar. 2016.

[4] R. Rincon, T. Fatoyinbo, K. J. Ranson, B. Osmanoglu, G. Sun, M. Deshpande, M. Perrine, C. D. Toit, Q. Bonds, J. Beck, and D. Lu, "The ecosystems SAR (EcoSAR) an airborne P-band polarimetric InSAR for the measurement of vegetation structure, biomass and permafrost," *IEEE Radar Conference*, pp. 1443–1445, May 2014.

[5] R. Rincon, T. Fatoyinbo, B. Osmanoglu, S. Lee, K. J. Ranson, G. Sun, M. Perrine, and C. D. Toit, "ECOSAR: P-band digital beamforming polarimetric and single pass interferometric SAR," *IEEE Radar Conference*, pp. 699–703, 2015.

[6] W. Weedon and R. Nunes, "Low-Cost Wideband Digital Receiver/Exciter (DREX) Technology Enabling Next-Generation All-Digital Phased Arrays," *IEEE Phased Array Systems and Technology Symposium*, 2016.

[7] G. Frazer, "Application of MIMO Radar Techniques to Over-the-Horizon Radar," *IEEE Phased Array Systems and Technology Symposium*, 2016.

[8] T. Mealey and A. Duly, "BEEMER: a firmware-tuned, software-defined MIMO radar testbed," *IEEE Phased Array Systems and Technology Symposium*, 2016.

[9] "IEEE Standard Letter Designations for Radar-Frequency Bands," *IEEE Std 521-1976*, pp. 1–8, Nov. 1976. DOI: 10.1109/IEEESTD.1976.7428784.

[10] M. A. Richards, *Fundamentals of Radar Signal Processing, 2nd Edition*. McGraw-Hill Education, 2005.

[11] T. Kouno and H. Onodera, "Consideration of transition-time variability in statistical timing analysis," in *2006 ieee international soc conference*, 2006, pp. 207–210. DOI: 10.1109/SOCC.2006.283882.

[12] M. Picciolo, J. Griesbach, and K. Gerlach, "Adaptive LFM Waveform Diversity," *2008 IEEE Radar Conference*, pp. 1–6, May 2008.

[13] D. Akos, M. Stockmaster, J. Tsui, and J. Caschera, "Direct bandpass sampling of multiple distinct rf signals," *Ieee trans. commun.*, vol. 47, no. 7, 983–988, Jul. 1999.

[14] C. Tseng and S. Chou, "Direct downconversion of multiband rf signals using bandpass sampling," *Ieee trans. wireless commun.*, vol. 5, no. 1, pp. 72–76, Jan. 2006.

[15] R. Vaughan, N. Scott, and D. White, "The theory of bandpass sampling," *Ieee trans. signal process.*, vol. 39, no. 9, 1973–1984, Sep. 1991.

[16] N. Wong and T. Ng, "An efficient algorithm for downconverting multiple bandpass signals using bandpass sampling," *In proc. ieee int. symp. circuits syst.*, vol. 3, 910–914, Jun. 2001.

[17] D. Linden, "A discussion of sampling theorems," *Proc. ire*, vol. 47, no. 7, 1219–1226, Jul. 1959.

[18] A. Kiyono, M. Kim, K. Ichige, and H. Arai, "Jitter effect on digital downconversion receiver with undersampling scheme," in *Circuits and systems, 2004. mwscas '04. the 2004 47th midwest symposium on*, vol. 2, 2004, II–677–80 vol.2.

[19] M. Mishali and Y. C. Eldar, "Sub-nyquist sampling," *Ieee signal processing magazine*, vol. 28, no. 6, pp. 98–124, Nov. 2011, ISSN: 1053-5888.

[20] L. Pierno, A. M. Fiorello, A. Secchi, and M. Dispenza, "Fibre optics in radar systems: Advantages and achievements," in *2015 ieee radar conference (radarcon)*, May 2015, pp. 1627–1633. DOI: 10.1109/RADAR.2015.7131259.

[21] M. Yeary, J. Meier, R. Kelley, and R. Palmer, "Compact digital receiver development for radar based remote sensing," *IEEE-IMTC*, pp. 1761–165, May 2008.

[22] T. Hosman, M. Yeary, and J. Antonio, "Design and characterization of an mfsk-based transmitter/receiver for ultrasonic communication through metallic structures," *Ieee transactions on instrumentation and measurement*, vol. 60, no. 12, Dec. 2011.

[23] W. Kester, *What the nyquist criterion means to your sampled data system design*, Analog Devices, 2009.

[24] R. P. S. Rathore, "Reconfigurable digital radar receiver implemented in FPGA using under-sampling, direct IQ generation, multi-rate filter and pulse compression," *2014 IEEE International Microwave and RF Conference (IMaRC)*, pp. 174–177, Dec. 2014.

[25] C.Shannon, "Communication in the Presence of Noise," *Procedings of the I.R.E*, pp. 10–11, Jan. 1949.

[26] S. K. Mitra, *Digital Signal Processing A Computer Base Approach, 4th Edition*. McGraw-Hill Education, 2006.

[27] P.Bloomfield, *Fourier analysis of time series: An introduction*. New York: Wiley-Interscience, 2000.

[28] F.Harris, "On the use of windows for harmonic analysis with the discrete fourier transform," *Proceedings of the IEEE*, vol. 66, pp. 51–83, Jan. 1978.

[29] J. Tukey, "An introduction to the calculations of numerical spectrum analysis," *Spectral Analysis of Time Series: 2546*, 1967.

Appendicies

A Waveform Generation Code

This code was used to generate the waveform samples that were uploaded to the FPGA communicating with the DAC. The code created the chirp desired and quantized the samples to 16 bits. The DAC samples were written to a csv file with each column corresponding to a channel on the DAC.

```
clc;
clear all;
close all;

%Create Waveform
fs=(1160/4)*1e6;
B=200e6;
T=2e-6;
N=fs*T;
N=floor(N/32)*32;
T=N/fs;
fc=0e6;
t=(0:N-1)/fs;
t=t-T/2;
k=B/2/T;
xsig=exp(1i*2*pi*k*t.^2);
x=real(xsig);
y=imag(xsig);

%Quantize Waveform
x=floor(x*((2^16-1)/2));
y=floor(y*((2^16-1)/2));
tempr=round(x.'*((2^16/2)-1));
tempi=round(y.'*((2^16/2)-1));
dacmem=8096;
bits(:,1)=[zeros(1,dacmem-(length(x)+91)),
x, zeros(1,91)];
bits(:,2)=[zeros(1,dacmem-(length(y)+91)),
y, zeros(1,91)];
bits(:,3)=[zeros(1,dacmem-(length(x)+91)),
x, zeros(1,91)];
bits(:,4)=[zeros(1,dacmem-(length(y)+91)),
y, zeros(1,91)];
```

```
%Plot Waveform
time=(0:length(bits)-1)/(fs*1e6);
plot(time,bits/((2^16/2)-1));
xlabel('Time(s)');
ylabel('Amplitude');
title(['20\musec LFM pulse with
\beta=' num2str(B*1e-6) 'MHz and
F_c=' num2str(fc*1e-6) 'MHz']);
figure();

%Write waveform File
fileID = fopen('text.txt','w');
for index=1:length(bits(:,1))
    fprintf(fileID,'%s','2b');
fprintf(fileID,'%s,',dec2bin(
typecast(int16(bits(index,1)),'uint16'),16));
end
fclose(fileID);
csvwrite('Real.csv',bits);

%Plot Analysis for waveform
Nfft=10e6;
plot(linspace(-.5,.5,Nfft)*fs*1e-6,
db(fftshift(fft(bits,Nfft))))
title(['Frequency Spectrum of 20\musec pulse
with \beta=' num2str(B*1e-6) 'MHz
and F_c=' num2str(fc*1e-6) 'MHz']);
xlabel('Frequency(MHz)');
ylabel('dB');
figure()
Nam=length(xsig);
tam=-(T/2):(T)/(Nam-1):(T/2);
about=ambig(length(xsig),xsig);
about(abs(about)>50)=-50;
dop=linspace(-0.5,0.5,2*length(xsig)-1)*fs*1e-6;
surface((tam)*1e6,dop,about);
axis([-.5 .5 -50 50])
shading flat;
title('Ambiguity of Chirp Waveform Used');
xlabel('Time Delay (\mus)');
ylabel('Doppler Frequency(Hz)');
```

B Predistortion Code

This is the Predistortion code that calculates the envelope characterized as the system response. The code then generates the predistortion to be applied to the waveform. The code then rewrites the predistorted waveform to be sent to the FPGA to be delivered to the DAC.

```
clc;
clear all;
close all;

%% Read in the received signal for predistortion
fs=580e6;
minval=15115;
signallen=1179;
maxval=minval+signallen;
a=csvread('Receivedsecond.csv');

%% Plot received signal and frequency spectrum
figure();
subplot(2,1,1);
time=(0:length(a)-1)/(fs);
plot(a./((2^12/2)-1));
xlabel('Time(s)');
axis([1.5e4 1.65e4 -1 1]);
ylabel('Amplitude');
title('Signal Received from ADC');
subplot(2,1,2);
Nfft=1e6;
freq=linspace(-.5,.5,Nfft)*fs;
spec=db(fftshift(fft(a(minval:maxval)
./max(a(minval:maxval)),Nfft)));
fftrecsig=fft(a(minval:maxval)
./max(a(minval:maxval)));
fftrecsig(1:3500)=0;
plot(freq,spec);
axis([-fs/2 fs/2 -40 50]);
title('Frequency Spectrum of
a Single Pulse from Received Signal');
xlabel('Frequency(MHz)');
ylabel('Amplitude');

%% Remove DC
```

```
sig=fft(a(minval:maxval,1));
sig(1)=0;
x=ifft(sig);
val=max(x);
x=x./max(x);

%% Estimate Envelope
A= envelope(x,80,'peak');
t=(0:length(x)-1)/(fs);
figure();
plot(t,x);
axis([0 max(t) -1 1]);
title('Envelope Estimation');
xlabel('Time(s)');
ylabel('Amplitude');
hold on
plot(t,A);
hold off
legend('Distorted Signal','Envelope'
,'Location','SouthEast');
env=A;
win=1./env;
win=win./max(win);

%% Get reference signal and apply predistortion
sig=csvread('Real.csv');
tt=1:length(sig(:,1));
rsig=resample(sig(7428:8017,1:2),2,1);
powertimerec=(0:length(a(minval:maxval))-1)/(fs);
powertimeref=(0:length(rsig)-1)/(fs);
normval=max(sig(:,1));
rsig=rsig./normval;
pds(:,1)=rsig(:,1).*win;
pds(:,2)=rsig(:,2).*win;
pds=pds./max(pds(:,1));
pdsnowin=resample(pds,1,2);
twindow=tukeywin(length(pds),0.1);
pdswin(:,1)=pds(:,1).*twindow;
pdswin(:,2)=pds(:,2).*twindow;
pdswin=resample(pdswin,1,2);
pds(:,1)=pds(:,1).*twindow;
pds(:,2)=pds(:,2).*twindow;
```

```
pds=pds./max(pds(:,1));
pds=floor(pds.*(2^16-1)/2);
pds=resample(pds,1,2);

%% Plot predistorted signal for analysis
figure()
tdis=(0:length(pds)-1)/(290*1e6);
plot(tdis,pds./((2.^16/2)-1));
axis([0 max(tdis) -1 1]);
title('Pre-distorted Signal');
xlabel('Time(s)');
ylabel('Amplitude');

%% Write Signal to file
dacmem=8096;
pds=[zeros(dacmem-(length(pds)+91),2);
pds ; zeros(91,2)];
figure()
prefft=fft(pds(:,1)./max(pds(:,1)));
plot(linspace(-0.5,0.5,length(pds))*fs
,db(fftshift(prefft)));
prefft(1:length(prefft)/2)=0;
title('Frequency Spectrum of
Pre-Distorted Signal');
xlabel('Frequency(MHz)');
ylabel('Amplitude');
pdso(:,1)=pds(:,1);
pdso(:,2)=pds(:,2);
pdso(:,3)=pds(:,1);
pdso(:,4)=pds(:,2);
csvwrite('Realdistort.csv',pdso);
```

C Ambiguity Function of Chirp Pulse

This code calculated the ambiguity function for a chirp pulse. The code generated the chirp pulse and produced the ideal matched filter. The code then calculated the output of the matched filter at varying time delays and Doppler shifts. The last section of the code extracts the zero Doppler and zero time delay cuts of the ambiguity function.

```
close all;
clear all;
clc;

%% Create Chirp
fs=(1160/4)*1e6;
B=200e6;
T=2e-6;
N=fs*T;
N=floor(N/32)*32;
T=N/fs;
fc=0e6;
t=(0:N-1)/fs;
t=t-T/2;
k=B/2/T;
xsig=exp(1i*2*pi*k*t.^2);

%% Perform Ambiguity
out=ambig(length(xsig),xsig);
out(abs(out)>50)=-50;

%% Plotting Routine
t=(0:(length(xsig)-1))/fs;
T=length(xsig)/fs;
time=t-T/2;
dop=linspace(-0.5,0.5,2*length(xsig)-1)*fs*1e-6;
subplot(2,1,1)
plot(time *1e6,xsig);
xlabel('Time (\mus)');
ylabel('Amplitude (V)');
title('Chirp Waveform');
figure();
subplot(2,1,1);
surface(time*1e6,dop.',out);
axis([-.5 .5 -50 50])
```

```
xlabel('Time (\mus)');
ylabel('Doppler (Hz)');
title('Ambiguity Function of Chirp Pulse');
colorbar;
shading flat;
subplot(2,1,2);
surface(time*1e6,dop.',out);
axis([-.5 .5 -50 50 -50 0]);
xlabel('Time (\mus)');
ylabel('Doppler (Hz)');
zlabel('Amplitude (dB)');
colorbar;
shading flat;

%% Plot Zero Doppler and Zero Time Delay Cuts
figure()
subplot(2,1,1);
plot(dop,out(:,floor(size(out,2)/2)));
title('Zero Time Delay Cut');
xlabel('Doppler Shift');
ylabel('Amplitude (dB)');
subplot(2,1,2);
plot(time*1e6,out(floor(size(out,1)/2),:));
title('Zero Doppler Shift Cut');
xlabel('Time Delay');
ylabel('Amplitude (dB)');
```

D Ambiguity Function

This is the function used in the previous code to generate the ideal matched filter and implementing the convolution of the signal with the matched filter. The function outputs the ambiguity values in matrix form.

```
function [out]=ambig(N,x)

%Create matched filter
C=convmtx(fftshift(fft(conj(x),N)),2*N-1);

% Pad signal for convolution
pad=[zeros(1,N-1) fftshift(fft(x,N)) zeros(1,N-1)];
for i=1:size(C,1)
    paded(i,:)=pad.';
end

% Apply frequency domain convolution
amb=paded.*C;
about=ifftshift(ifft(amb(:,N:N+N-1),N,2),2);

% Output of matched filter in dB
out=20*log10(abs(about)/max(abs(about(:))));
end
```

E Coherent Integration of Range Targets

This is the code used to extract the targets shown in the range test. The code created the matched filter from the loopback test and then creates a complex signal by removing the left image of the frequency spectrum. The matched filter then is generated by taking the inverse fft of the remaining spectrum.

```
clear all;
close all;
clc;

%% Create Matched Filter
c=299792458;
x=csvread('matchfilt.csv');
fs = 580e6;
N=fs*2e-6;
h=x(3025+[0:N-1])/2^16;
Nfft=length(h);
w=linspace(-0.5,0.5,Nfft)*fs;
H=fft(h,Nfft);
H(length(H)/2:end)=-eps;
win=ones(1,N)*-eps;
win(127:579)=max(H);
H=H.*win;
hmf=ifft(H);

%% Read Files and Apply Matched Filter
files = {'maxpow_notarg1.csv',
'cornerreflect_maxpow_halfdist.csv' ,
'cornerreflect_maxpow.csv'};
titles = {'No Target',
'Corner Reflectors at 120m and 140m',
'Corner Reflectors at 120m and 160m'};
for j=1:length(files)
y=csvread(files{j});
ind=y(:,2)./max(y(:,2));
[ind,~]=find(ind==1);
[ind2,~]=find(diff(ind)~=1);
ind=ind(ind2);

if all(diff(ind))==2^12
    warning('PRF not constant')
else
```

```
for i=1:length(ind)
    ph(i,:)=y(ind(i)+[0:2048],1)/2^16;
    mf2(i,:)=conv(conj(fliplr(hmf)),ph(i,:));
end
end
t=[0:size(mf2,2)-1]/fs;

%% Plot the mean of all the pulses
%%(Coherent integration)
subplot(3,1,j)
plot(t*c/2,db(mean(abs(mf2)),1));
title(titles{j})
xlabel('Range(m)')
ylabel('dB')
xlim([0 360])
ylim([-95 -60])
end
```

F Range Doppler Code

This code is the code used to generate the range Doppler map shown in the paper. The code creates and applies the matched filter and then plots the range profile of the target scene. Lastly, the code creates the range Doppler map by performing the additional fft to extract the Doppler frequency.

```
clear all
close all
clc

%% Create Matched Filter
c=299792458;
x=csvread('MatchedFilter.csv');
fs = 580e6;
N=fs*2e-6;
h=x(3033+[0:N-1])/2^16;
Nfft=length(h);
w=linspace(-0.5,0.5,Nfft)*fs;
H=fft(h,Nfft);
H(length(H)/2:end)=-eps;
win=ones(1,N)*-eps;
win(127:579)=max(H);
H=H.*win;
t=[0:N-1]/fs;
hmf=ifft(H);

%% Read Data File
y=csvread('CPPar_rotation1_Broad.csv');
uint32 ind;
uint32 k;
uint32 j;
ind=y(:,2)./max(y(:,2));
[ind,~]=find(ind>0.9);
[ind2,~]=find(diff(ind)~=1);
ind=ind(ind2);

%% Apply Matched Filter
matchfilter=fft(conj(hmf(end:-1:1)),3001);
ph=zeros(65535,3001);
for j=2:length(ind)
    ph(j,:)=y(ind(j)+[0:3000]-580,1)/2^16;
end
```

```
parfor k=2:length(ind)
    tempf=fft(ph(k,:),3001).*matchfilter;
    tempt=ifft(tempf);
    mf(k,:)=tempt(580:end);
end

%% Plot Range measurements and Range Doppler Map
t=[0:size(mf,2)-1]/fs;
plot(t*c/2-14,db(mean(abs(mf),1)))
title('Averaged')
xlabel('Range(m)')
ylabel('dB')
ylim([-100 -40])
figure()
plot(t*c/2,db(mf(7,:)))
title('1 Pulse')
xlabel('Range(m)')
ylabel('dB')
ylim([-100 -40])
figure();
PRI=3000/580e6;
PRF=1/PRI;

%% Create Range Doppler
Range=(((0:length(1250:1600)-1)+1249)/fs)*c/2-24;
Doppler=-PRF/2:PRF/(100*1499-1):PRF/2;
Image=db(fftshift(fft(mf(:,1250:1600),100*1499,1),1));
imagesc(Range,Doppler,Image);
axis([300 380 -80 80]);
xlabel('Range(m)');
ylabel('Doppler Shift(Hz)');
title(' Range Doppler of Area Near the Target');
colorbar;
```